HDL-TR-1711

ELECTROMAGNETIC PULSE COUPLING WITH LOSSLESS MULTICONDUCTOR TRANSMISSION LINES

JUNE 1975

THIS WORK IS SPONSORED BY
THE DEFENSE NUCLEAR AGENCY UNDER SUBTASK R99QAXEB075-42.
WORK UNIT TITLE MULTICONDUCTOR TRANSMISSION LINES.

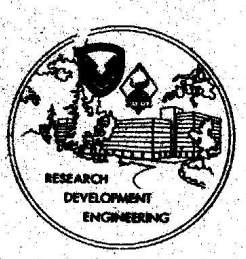

U.S. Army Materiel Command
HARRY DIAMOND LABORATORIES
Adelphi, Maryland 20783

The findings in this report are not to be construed as an official Department of the Army position unless so designated by other authorized documents.

Citation of manufacturers' or trade names does not constitute an official indorsement or approval of the use thereof.

Destroy this report when it is no longer needed. Do not return it to the originator.

UNCLASSIFIED

SECURITY CLASSIFICATION OF THIS PAGE *(When Data Entered)*

REPORT DOCUMENTATION PAGE		READ INSTRUCTIONS BEFORE COMPLETING FORM
1. REPORT NUMBER HDL-TR-1711	2. GOVT ACCESSION NO.	3. RECIPIENT'S CATALOG NUMBER
4. TITLE *(and Subtitle)* Electromagnetic Pulse Coupling with Lossless Multiconductor Transmission Lines		5. TYPE OF REPORT & PERIOD COVERED Technical Report 6. PERFORMING ORG. REPORT NUMBER
7. AUTHOR(s) Janis Klebers		8. CONTRACT OR GRANT NUMBER(s) NWER Subtask R99QAXEB075-42
9. PERFORMING ORGANIZATION NAME AND ADDRESS Harry Diamond Laboratories 2800 Powder Mill Road Adelphi, MD 20783		10. PROGRAM ELEMENT, PROJECT, TASK AREA & WORK UNIT NUMBERS EB075
11. CONTROLLING OFFICE NAME AND ADDRESS Director Defense Nuclear Agency Washington, DC 20305		12. REPORT DATE June 1975 13. NUMBER OF PAGES 48
14. MONITORING AGENCY NAME & ADDRESS*(if different from Controlling Office)*		15. SECURITY CLASS. *(of this report)* Unclassified 15a. DECLASSIFICATION/DOWNGRADING SCHEDULE

16. DISTRIBUTION STATEMENT *(of this Report)*

Approved for public release; distribution unlimited.

17. DISTRIBUTION STATEMENT *(of the abstract entered in Block 20, if different from Report)*

18. SUPPLEMENTARY NOTES

This work was sponsored by the Defense Nuclear Agency under Subtask R99QAXEB075-42, Work Unit Title "Multiconductor Transmission Lines."

Data and work presented in this report were completed during FY74.

19. KEY WORDS *(Continue on reverse side if necessary and identify by block number)*

EMP
Transmission lines
Electromagnetic coupling
Cables
Multiconductor transmission lines
Distributed excitation of transmission lines

20. ABSTRACT *(Continue on reverse side if necessary and identify by block number)*

The matrix formulation of the transmission line equations was applied in a semi-empirical manner to predict electromagnetic coupling with multiconductor transmission lines. Experimental procedures were used for measuring characteristic electrical parameters for transmission lines. The NLINE multiconductor transmission line computer program was used with experimental data for analysis of transmission-line samples made up of 2, 3, and 11 conductors. Parametric variations in angle of incidence and

DD FORM 1 JAN 73 1473 EDITION OF 1 NOV 65 IS OBSOLETE

UNCLASSIFIED

SECURITY CLASSIFICATION OF THIS PAGE *(When Data Entered)*

transmission line parameters were studied and compared with experimental results. The validity of simplifying approximations was checked with experimental data.

CONTENTS

ILLUSTRATIONS

ILLUSTRATIONS (CONT'D)

1. INTRODUCTION

The interaction of electromagnetic fields with transmission lines has been a subject of interest in many applications in nuclear electromagnetic pulse (EMP) technology. This report presents numerical and experimental results on EMP coupling with unshielded, lossless multiconductor transmission lines. A semi-empirical approach was developed combining basic transmission line theory with experimental and digital computer techniques that can be applied to relatively complex geometries. For the most part, the supporting theory is contained in standard texts on transmission lines. Traditionally, the theory has been formulated in the frequency domain. Corresponding results have been obtained in the time domain principally by numerical Fourier transform methods. A set of equations is written in matrix form to describe the electrical response of the transmission line. Methods developed in this study are based for the most part on a formulation contained in the work by Frankel.[1]

2. TYPES OF TRANSMISSION LINES CONSIDERED

Electromagnetic waves propagate along systems of conductors and dielectrics that can be either intentional or unintentional transmitters of energy. The model of the multiconductor transmission line considered in this report is defined as any configuration of parallel, unshielded, lossless conductors, uniform in cross section in the axial direction, and surrounded by free space or by a homogeneous isotropic dielectric material. A free space permeability μ_o is assumed. A perfectly conducting ground plane can be added in the presence of the conductors when needed for the problem. Figure 1 shows cross sections of typical transmission lines that can be analyzed.

3. THE GEOMETRY AND SYSTEM OF COORDINATES

Figure 2 shows a representative transmission line with the selected coordinates and directions of EMP incidence. A convenient conductor is chosen as a reference, and differential voltages and currents are computed on the remaining conductors with respect to the reference.

---

[1] *Sidney Frankel, Cable and Multiconductor Transmission Line Analysis, Harry Diamond Laboratories TR-091-1 (28 June 1974).*

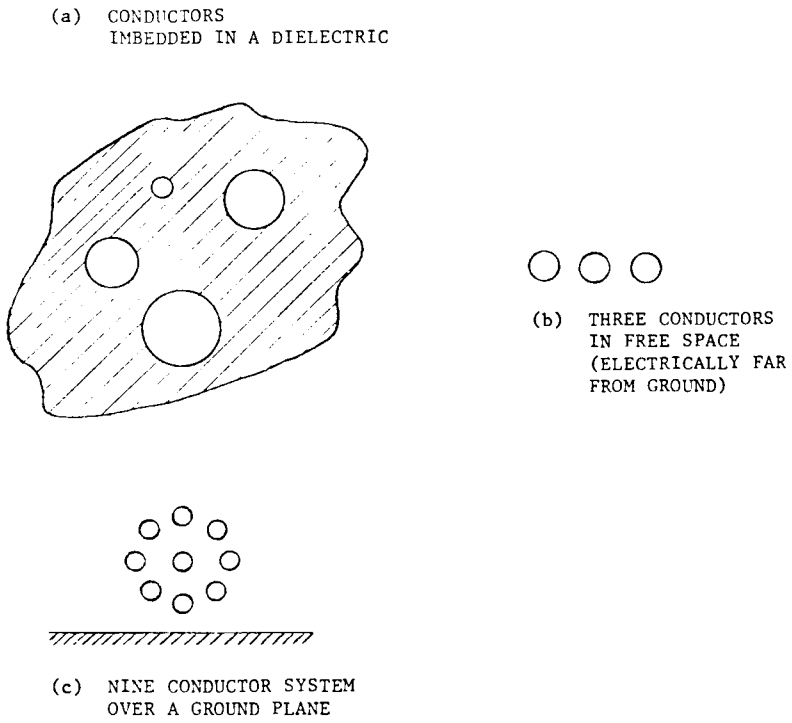

Figure 1. Examples of multiconductor transmission lines.

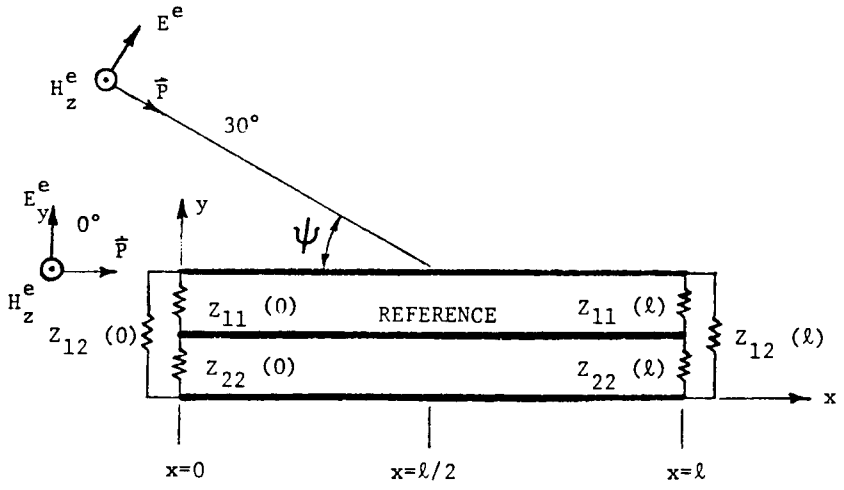

Figure 2. Typical geometry for the transmission line.

The x-axis is always chosen in the direction parallel to the axial direction of the conductors in this report. Results obtained at $x = 0$ represent node voltages and currents at the left-hand load impedances in figure 2. Correspondingly, node voltages and currents at the right-hand load impedances are obtained when x is set equal to ℓ, the length of the transmission line. Induced voltages and currents at any other point along the transmission line can be obtained when x is set equal to the desired value within the limits $0 \leq x \leq \ell$.

The acute angle formed between Poynting's vector $\vec{P}$ of the incident plane wave and the longitudinal x-axis of the transmission line defines the angle of incidence ψ in figure 2. This angle is varied between the limits $0 \leq \psi \leq 90$ deg.

An additional change in geometry can be introduced by rotation of the transmission line about its longitudinal x-axis with respect to the incident wave. This rotation is equivalent to a change in the polarization of the incident wave with respect to the transmission line.

The terminating impedances $Z_{ij}(0)$ and $Z_{ij}(\ell)$ can be of arbitrary value and are chosen to be real in computational examples contained in this report.

4. ASSUMPTIONS FOR THE TEM RESPONSE IN THE TRANSMISSION LINE

Several mechanisms of interaction and coupling are present when an electromagnetic wave impinges on the transmission line. Some portion of the incident energy is scattered off the conductors. The cable response in both the differential (transmission line) and the common (antenna) modes. When the conductor diameters are similar in size, are small compared to wavelength, and are spaced such that no appreciable shielding is present between conductors, the induced common mode currents and voltages are assumed to be approximately the same on each conductor, tending to cancel in the terminating loads. Under such conditions, the common-mode coupling is neglected for the computation of the differential currents and voltages in the transmission line. The response is assumed to be entirely due to the transverse electromagnetic (TEM) mode, induced by the transverse components of the impressed electric and magnetic fields. The impressed fields are defined as the fields that would exist over the space occupied by the transmission line if the conductors were removed. Electromotive force (emf) is induced and acts as a distributed source on the conductors.

The conductors are assumed to be lossless, with constant cross section in the axial direction. The conductor diameters are assumed to be small compared to conductor spacings. The medium surrounding the conductors is either free space or a lossless, homogeneous, isotropic dielectric, with free space permeability μ_o and permittivity ε.

5. APPLICATION OF THE TRANSMISSION LINE EQUATIONS TO A SYSTEM OF MANY CONDUCTORS

The differential equations obtained for the parallel plate or the two-conductor transmission line are applied to more complex lines made up of many conductors by use of the matrix formulation. The order of the matrices for an N conductor transmission line is N-1, with one conductor chosen as a voltage and current reference. For N = 3 (e.g., two conductors over a ground plane), the equations are

$$\left.\begin{aligned} \frac{d}{dx}\begin{bmatrix} V_1 \\ V_2 \end{bmatrix} + j\omega \begin{bmatrix} L_{11} & L_{12} \\ L_{21} & L_{22} \end{bmatrix} \begin{bmatrix} I_1 \\ I_2 \end{bmatrix} &= j\omega H_z^e \begin{bmatrix} L_1^e \\ L_2^e \end{bmatrix} \\ \frac{d}{dx}\begin{bmatrix} I_1 \\ I_2 \end{bmatrix} + j\omega \begin{bmatrix} C_{11} & C_{12} \\ C_{21} & C_{22} \end{bmatrix} \begin{bmatrix} V_1 \\ V_2 \end{bmatrix} &= j\omega E_y^e \begin{bmatrix} C_1^e \\ C_2^e \end{bmatrix} \end{aligned}\right\} \qquad (1)$$

With matrix quantities underlined, the general forms are

$$\left.\begin{aligned} \frac{d\underline{V}}{dx} + j\omega \underline{L}\,\underline{I} &= j\omega H_z^e \underline{L}^e \\ \frac{d\underline{I}}{dx} + j\omega \underline{C}\,\underline{V} &= j\omega E_y^e \underline{C}^e \end{aligned}\right\} \qquad (2)$$

The impressed magnetic field H_z^e and the impressed electric field E_y^e are the transverse components of the electromagnetic field in the medium surrounding the conductors.

$\underline{V}$ and $\underline{I}$ are column matrices of length N-1 representing voltages and currents on each conductor measured with respect to the reference.

$\underline{C}$ is an N-1 by N-1 symmetric matrix defining the Maxwell's capacitance coefficients for the conductors.[1,2]

$\underline{L}$ is an N-1 by N-1 symmetric matrix defining the inductance coefficients for the conductors. These coefficients are obtained from the inverse of the capacitance matrix and the propagation velocity v of the transmission line:

$$\underline{L} = \frac{1}{v^2} \underline{C}^{-1} \tag{3}$$

$\underline{L}^e$ and $\underline{C}^e$ are column matrices of length N-1 and are referred to as the magnetic and electric field coupling parameters. Unlike the capacitance and inductance coefficients, which are functions only of the conductor configuration, the field coupling parameters depend both on the conductor cross section and on the incidence angle of the impressed fields. These parameters are obtained by use of Faraday's law between each conductor and the reference. Application of Faraday's law determines the values of the effective distributed voltage and current sources induced on the transmission line by the impressed fields. For most geometries, $\underline{L}^e$ and $\underline{C}^e$ must be determined by experiment or by approximation.[1]

ω is the radian frequency and $j = \sqrt{-1}$.

Solutions to equation (2) can be obtained by standard techniques. The resulting expressions for $\underline{V}$ and $\underline{I}$ are too lengthy to be included explicitly in this report, but are contained in Frankel's report.[1] The NLINE computer program was written to evaluate $\underline{V}$ and $\underline{I}$ in both the frequency and the time domains for a generalized multiconductor transmission line, with allowance for parametric variations of geometric and electrical properties.

---

[1] *Sidney Frankel, Cable and Multiconductor Transmission Line Analysis, Harry Diamond Laboratories TR-091-1 (28 June 1974), 30; 352-401; 140.*

[2] *S. Ramo and J. R. Whinnery, Field and Waves in Modern Radio, John Wiley & Sons, Inc., New York (1964), 264-265.*

6. DEFINITION OF THE IMPRESSED ELECTROMAGNETIC FIELDS

The two exponential pulse characteristics are assumed for the impressed fields. The time domain expressions are

$$\left.\begin{aligned} E_y^e(t) &= A(e^{-\alpha_1 t} - e^{-\alpha_2 t})/(e^{-\alpha_1 t_o} - e^{-\alpha_2 t_o}) \\ H_z^e(t) &= (\mu_o/\varepsilon)^{-\frac{1}{2}} E_y^e(t) \end{aligned}\right\} \tag{4}$$

where $t_o = \ell n(\alpha_2/\alpha_1)/(\alpha_2-\alpha_1)$ defines the zero to peak rise time of the pulse. The constants α_1 and α_2 determine the pulse duration and rise time, respectively. The peak amplitude of the impressed electric field is given by A in volts per meter. The frequency domain characteristics are defined by the Fourier transform of equation (4):

$$\begin{aligned} E_y^e(\omega) &= A(\alpha_2 - \alpha_1)/\{(j\omega + \alpha_1)(j\omega + \alpha_2)(e^{-\alpha_1 t_o} - e^{-\alpha_2 t_o})\} \\ H_z^e(\omega) &= (\mu_o/\varepsilon)^{-\frac{1}{2}} E_y^e(\omega) \end{aligned} \tag{5}$$

7. DETERMINATION OF $\underline{L}^e$, $\underline{C}^e$, $\underline{C}$, $\underline{L}$

The capacitive and inductive parameters determine the magnitude and distribution of charges induced by the impressed field on each conductor of the transmission line. Interaction of voltages and currents between conductors is fundamentally determined by self and mutual capacitances defined by Maxwell's capacitance coefficients $\underline{C}$. The response to the impressed field is introduced through the external field coupling parameters $\underline{L}^e$ and $\underline{C}^e$ and depends on both the conductor cross section and the incidence and polarization angles of the field.

Maxwell's capacitance coefficients $\underline{C}$ and magnetic field coupling parameters $\underline{L}^e$ are chosen as the independent variables. The inductive coefficients $\underline{L}$ and the electric field coupling parameters $\underline{C}^e$ are computed from them. Analytical solutions for the coefficients can be obtained from Laplace's equation. The solution of Laplace's equation is practical only for simple geometries. Since most geometries are complex, these parameters must be measured or computed from

approximations. A parallel plate transmission line facility (PPF) shown in figures 3, 4, and 5 was built to measure the cable parameters. Figure 4 shows the continuous wave (CW) configuration designed to measure $\underline{L}_e$ for a transmission line test sample.

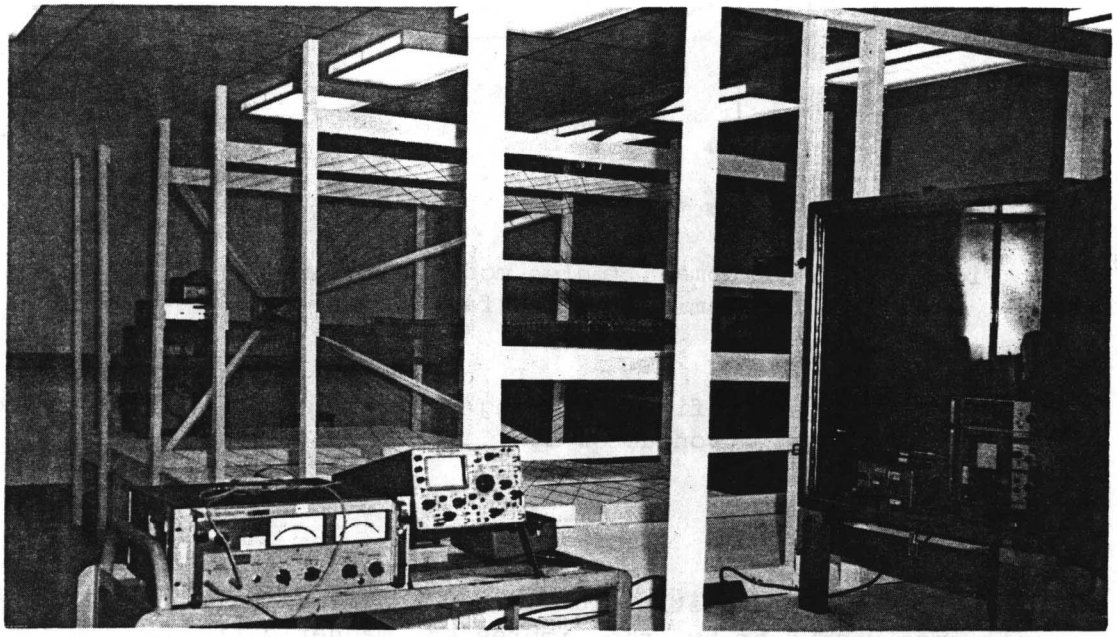

Negative No. 49-186-385-1974

Figure 3. The parallel plate transmission line facility.

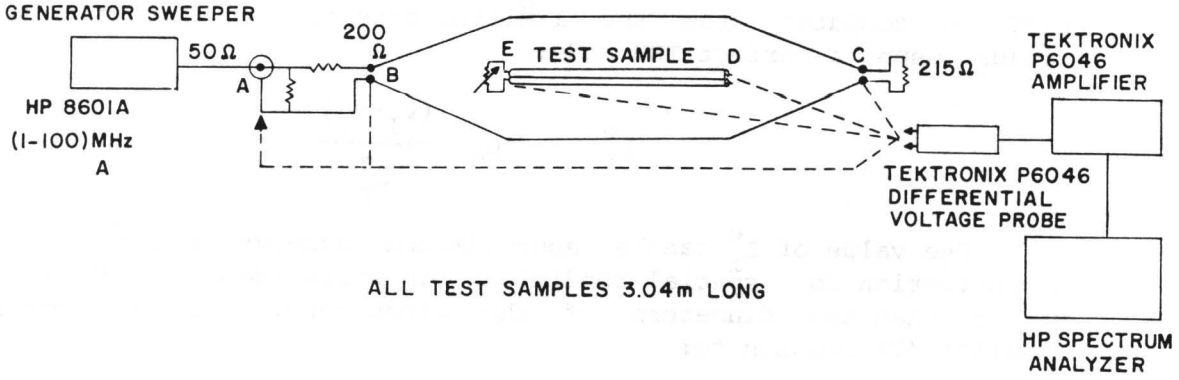

Figure 4. Experimental validation of analytical techniques: parallel plate transmission line facility.

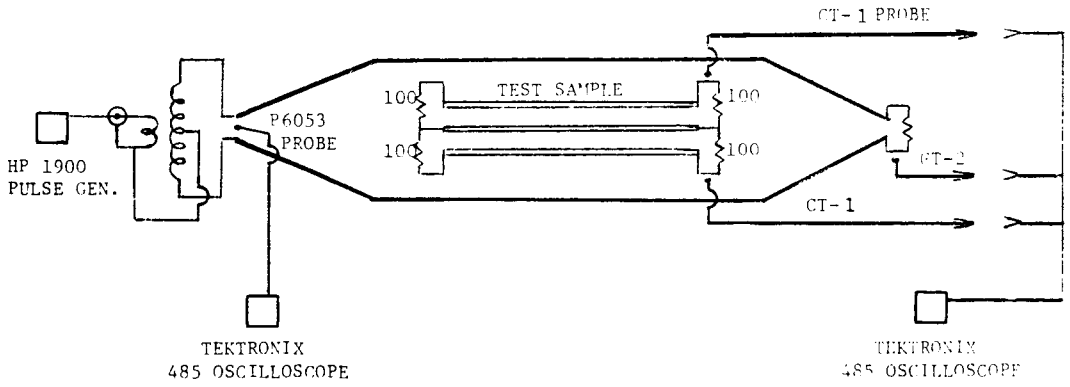

Figure 5. Time domain (pulse mode) operation of the parallel plate transmission line facility.

The magnetic field coupling parameters are inductive constants defined for the i^{th} conductor by

$$\phi_i = L_i^e H_y^e \tag{6}$$

where ϕ_i is the magnetic flux induced between the i^{th} conductor and the reference conductor by the impressed magnetic field. The value of L_i^e for each conductor depends on the cross section of the transmission line in the transverse plane and on the orientation of the impressed field. For measurement of L_i^e, the test sample is placed in a transverse electromagnetic field with all conductors open at the ends. The differential voltage v_i is measured on each conductor with respect to the reference conductor voltage v_o. The magnetic field coupling parameter is computed from the limiting condition in which the impressed fields assume a perfect TEM mode:

$$L_i^e \rightarrow \mu_o \frac{(v_i - v_o)}{E_y^e} \tag{7}$$

The value of L_i^e can be approximated accurately by the thin wire approximation for special conditions, in which the conductor spacing is greater than the diameters of the conductors. For such conditions, equation (7) reduces to:

$$L_i^e \simeq \mu_o h_i \tag{8}$$

where h_i is the distance measured along the electric-field line between the reference conductor and the i^{th} conductor. Figure 6 shows the results measured at two frequencies in the PPF for two parallel pipes, 4-in. diameter, separated at an increasing spacing. The measured value of L_2^e follows the thin wire limit after slight separation between the conductors. The measured value, however, remains below the thin wire limit.

Maxwell's capacitance coefficients complete the electrical description of the transmission line. The values can be determined by several methods: by analytical or numerical solution to Laplace's equation, by measurement, or by thin wire approximations. Because analytical and numerical solutions become prohibitively complex as the number of conductors is increased, they were not considered in this study.

The capacitance coefficients were measured for several test samples by an R-L-C capacitance meter. The self capacitances C_{ii} can be measured accurately by the meter. The R-L-C meter was not accurate enough to measure mutual capacitance.

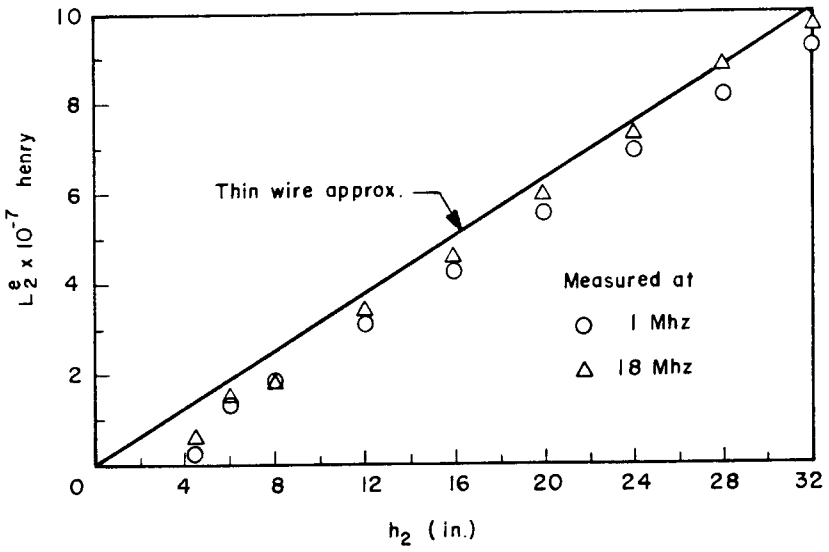

Figure 6. Comparison of measured and computed magnetic field coupling parameter for two parallel 4-in. diameter conductors separated by h_2.

The thin wire approximation was found to give acceptable results. The capacitance matrix is computed from the potential coefficients p_{ij} for the conductor configuration:

$$p_{ij} = \frac{1}{2\pi\epsilon} \ln \left[\frac{r_{i,o}\, r_{o,j}}{r_{i,j}\, r_{o,o}} \right] \tag{9}$$

where $r_{i,j}$ is the spacing between the centers of the i^{th} and j^{th} conductors for $i \neq j$, and r_{ii} is the radius of the i^{th} conductor. The matrix $\underline{p}$ is an N-1 by N-1 symmetric matrix. The capacitance matrix is determined from the inverse of $\underline{p}$:

$$\underline{C} = \underline{p}^{-1} \tag{10}$$

The remaining coupling parameters $\underline{C}^e$ and $\underline{L}$ are determined completely from $\underline{L}^e$ and $\underline{C}$.[1]

8. TRANSMISSION LINE TEST SAMPLES

Two multiconductor transmission lines were constructed for testing from coaxial cables with shields removed and dielectrics left around each conductor for spacing. One cable (sample A) is made from three (N = 3) RG-218 cables with shields removed. The second transmission line (sample B) is made up of 11 conductors (N = 11) from an assortment of cables. Figure 7 shows an end view of the two test samples in the open circuit condition. The shield of conductor 6 in sample B is taken as the sixth conductor in the transmission line. No measurements were taken on the center conductor of 6.

That the polyethylene surrounding the conductors changes the propagation velocity to 70 percent of the free-space value in sample A indicates an effective dielectric constant of 2.04. Measurements on sample B indicate the presence of a non-TEM mode due to an observed variation in propagation velocity ranging from 70 percent for conductors 1 and 2 to 76 percent for conductors 7 and 10. The resulting average dielectric constant is 1.89 for sample B.

The cross section of sample A is shown in figure 8. Terminating 100-ohm resistances were connected as shown at both ends of the transmission line. The coupling parameter matrices are included in figure 8. The capacitance matrix has been computed from the potential coefficients. The magnetic-field-coupling parameters have been

---

[1] *Sidney Frankel, Cable and Multiconductor Transmission Line Analysis, Harry Diamond Laboratories TR-091-1 (28 June 1974), 36,371.*

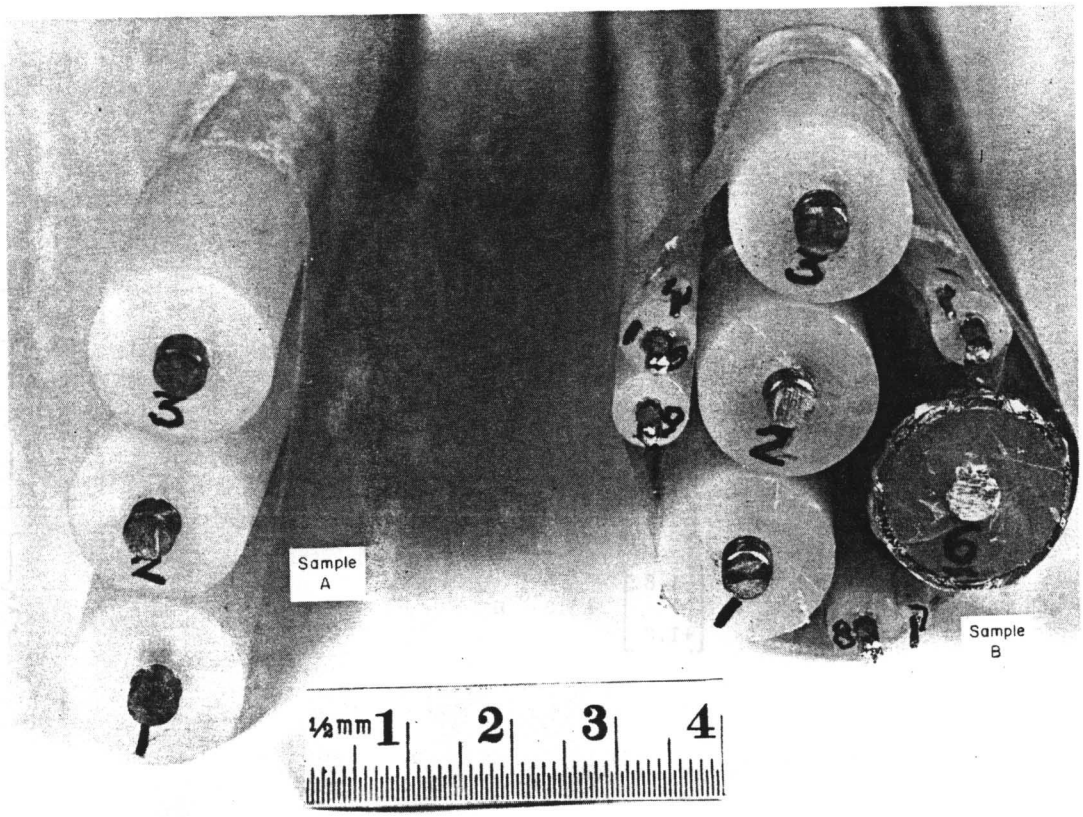

Negative No. 49-186-385-1974

Figure 7. End view of unterminated test samples.

determined from the thin wire approximation defined by equation (8). The corresponding measured values also are included. The conductors have been renumbered so that the implied subscripts in the matrices correspond to the proper conductor in sample A.

The measured and computed self capacitance values show close agreement. The measured values for the mutual capacitances tend to be larger in absolute value than the computed results in both test samples. The measurement technique does not appear to be accurate for these parameters.

The values for the magnetic field coupling parameter determined from the thin wire approximation are larger than the experimentally obtained values. This trend is in agreement with the results from the two-conductor experiment.

From potential coefficients:

$$\underline{C} = \begin{bmatrix} 31.9 & -10.3 \\ -10.3 & 31.9 \end{bmatrix} \quad \text{pF/m}$$

From thin-wire approximation:

$$\underline{L}^e = \begin{bmatrix} -2.14 \\ +2.14 \end{bmatrix} \times 10^{-8} \text{ H}$$

Measured values:

$$\underline{C} = \begin{bmatrix} 30 & -20 \\ -20 & 28 \end{bmatrix} \quad \text{pF/m}$$

$$\underline{L}^e = \begin{bmatrix} -1.8 \\ +1.8 \end{bmatrix} \times 10^{-8} \text{ H}$$

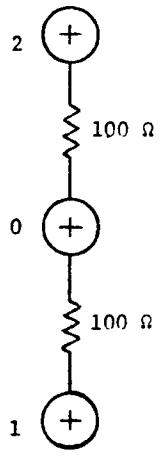

Scale:

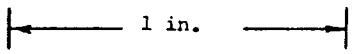

Figure 8. Sample A: measured and computed coupling parameters.

The cross section of sample B is shown in figure 9. The conductors have been renumbered to correspond to the matrix subscripts, with the reference conductor designated by 0. The capacitance matrix was determined by measurement and by computation from the potential coefficients. Values obtained by both methods for the self capacitance of each conductor are listed in figure 9. Because the measured off-diagonal terms were too large, they could not be used in the computations. Results from the potential coefficients indicate that

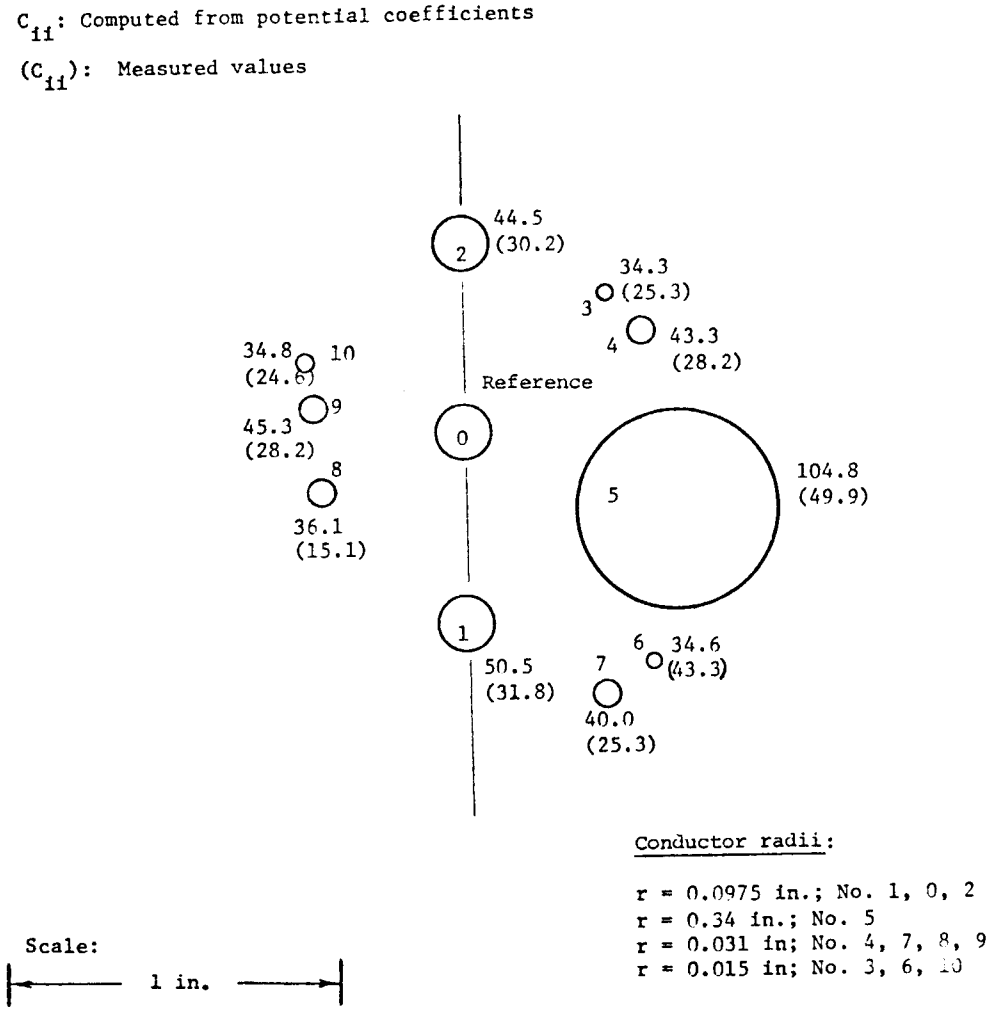

Figure 9. Sample B: comparison of computed and measured self capacitance coefficients (pF/m).

these terms should be approximately an order of magnitude less than self capacitances, or in the range of picofarads per meter or less, for most terms in sample B. The measurement by the R-L-C meter is not accurate to this order. Therefore, for computation, the potential coefficient method was used to determine the capacitance matrix. Figure 10 lists the matrix and its inverse for sample B.

Measured and computed magnetic field coupling parameters are given in figure 11 for sample B. In general, the values obtained from the thin wire approximation are larger than those measured in the PPF. This difference in the values is most likely due to conductor proximity effects in the test sample. The orientation of the impressed electric and magnetic fields, important for these measurements, is shown in figure 11.

(a) $\underline{C}$ computed from the potential coefficients for sample B (F/m)

$$
\begin{bmatrix}
.505E-10 & -.121E-11 & -.330E-13 & 0. & -.156E-10 & -.250E-11 & -.112E-10 & -.939E-11 & -.209E-11 & -.102E-11 \\
-.121E-11 & .445E-10 & -.872E-11 & -.479E-11 & -.759E-11 & -.658E-13 & -.626E-12 & -.185E-11 & -.408E-11 & -.627E-11 \\
-.330E-13 & -.872E-11 & .344E-10 & -.165E-10 & -.591E-11 & 0. & 0. & -.159E-12 & -.289E-12 & -.360E-12 \\
0. & -.479E-11 & -.165E-10 & .433E-10 & -.213E-10 & 0. & 0. & -.758E-13 & -.218E-12 & -.302E-12 \\
-.156E-10 & -.759E-11 & -.591E-11 & -.213E-10 & .105E-09 & -.195E-10 & -.128E-10 & -.216E-11 & -.111E-11 & -.116E-11 \\
-.250E-11 & -.658E-13 & 0. & 0. & -.195E-10 & .346E-10 & -.148E-10 & -.265E-12 & -.163E-12 & -.124E-12 \\
-.112E-10 & -.626E-12 & 0. & 0. & -.128E-10 & -.148E-10 & .400E-10 & -.775E-12 & -.423E-12 & -.330E-12 \\
-.939E-11 & -.185E-11 & -.159E-12 & -.758E-13 & -.216E-11 & -.265E-12 & -.775E-12 & .361E-10 & -.105E-10 & -.242E-11 \\
-.209E-11 & -.408E-11 & -.289E-12 & -.218E-12 & -.111E-11 & -.163E-12 & -.423E-12 & -.105E-10 & .453E-10 & -.191E-10 \\
-.102E-11 & -.627E-11 & -.360E-12 & -.302E-12 & -.116E-11 & -.124E-12 & -.330E-12 & -.242E-11 & -.191E-10 & .348E-10
\end{bmatrix}
$$

(b) Inverse of $\underline{C}$ computed by NLINE

$$
\begin{bmatrix}
.376E+11 & .136E+11 & .155E+11 & .173E+11 & .197E+11 & .257E+11 & .271E+11 & .175E+11 & .138E+11 & .136E+11 \\
.136E+11 & .367E+11 & .223E+11 & .206E+11 & .159E+11 & .173E+11 & .164E+11 & .125E+11 & .150E+11 & .173E+11 \\
.155E+11 & .223E+11 & .548E+11 & .338E+11 & .208E+11 & .216E+11 & .198E+11 & .120E+11 & .127E+11 & .141E+11 \\
.173E+11 & .206E+11 & .338E+11 & .503E+11 & .240E+11 & .246E+11 & .225E+11 & .126E+11 & .128E+11 & .140E+11 \\
.197E+11 & .159E+11 & .208E+11 & .240E+11 & .288E+11 & .291E+11 & .262E+11 & .129E+11 & .120E+11 & .127E+11 \\
.257E+11 & .173E+11 & .216E+11 & .246E+11 & .291E+11 & .652E+11 & .415E+11 & .160E+11 & .143E+11 & .149E+11 \\
.271E+11 & .164E+11 & .198E+11 & .225E+11 & .262E+11 & .415E+11 & .572E+11 & .163E+11 & .142E+11 & .147E+11 \\
.175E+11 & .125E+11 & .120E+11 & .126E+11 & .129E+11 & .160E+11 & .163E+11 & .410E+11 & .193E+11 & .171E+11 \\
.138E+11 & .150E+11 & .127E+11 & .124E+11 & .120E+11 & .143E+11 & .142E+11 & .193E+11 & .408E+11 & .277E+11 \\
.136E+11 & .173E+11 & .141E+11 & .140E+11 & .127E+11 & .149E+11 & .147E+11 & .171E+11 & .277E+11 & .495E+11
\end{bmatrix}
$$

Figure 10. Maxwell's capacitance coefficient matrix $\underline{C}$ and its inverse.

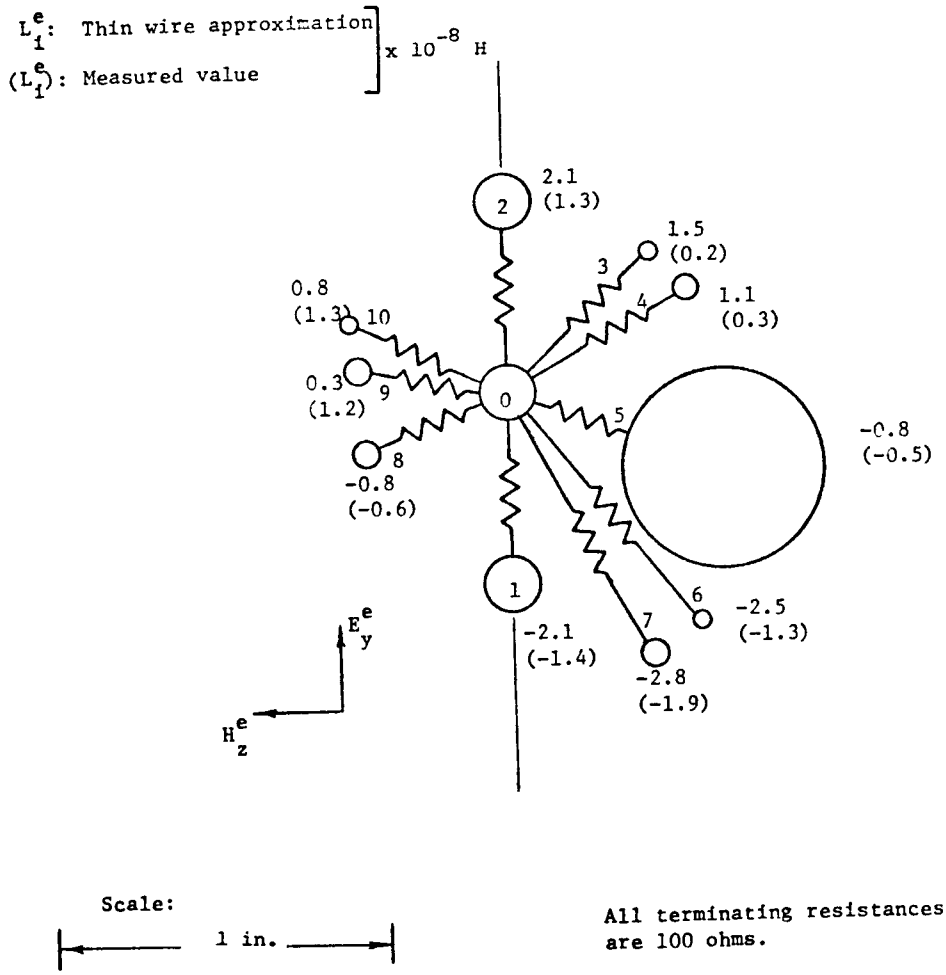

Figure 11. Sample B: thin wire approximation and the measured values for $\underline{L}^e$.

The configuration of conductors 1, 0, and 2 in sample B is identical to that in sample A. The addition of the eight conductors to the original three changes the computed self capacitance of conductors 1 and 2 from 31.9 pF/m to values of 50.5 and 44.5 pF/m. Thus, the effects on self capacitance due to the addition of neighboring conductors are observed by a study of the two samples. The measured values, however, do not show as much of a change. The measured values of the magnetic-field-coupling parameters L_1^e and L_2^e are lowered from 1.8 x 10^{-8} H to ~1.4 x 10^{-8} H with addition of the eight conductors. This lowering indicates a shielding effect on conductors 1 and 2. This effect is observed only experimentally, and not by use of the thin wire approximation, where proximity effects are neglected.

Figure 11 lists the measured and computed magnetic field coupling parameters for sample B. The values obtained from the thin wire approximation are, for all conductors but two (9 and 10), larger than those obtained by measurement. This result is most likely due to proximity effects in the test sample. Also, the orientation of the impressed electric and magnetic fields is shown in figure 11, since $\underline{L}^e$ can change with the polarization angle.

The magnetic field coupling parameters were measured under open circuit conditions. For convenience, figure 11 shows the manner in termination of sample B with 100-ohm resistances for subsequent induced current and voltage measurements and computations.

9. NUMERICAL AND EXPERIMENTAL RESULTS

The PPF was operated in the time domain (pulse mode, as shown in figure 5) to excite the sample transmission lines with a simulated plane wave, incident end-on at ψ = 0 deg. Tektronix current probes were used to measure induced current at the loads for both samples. A comparison of the measured impressed field waveshape and the measured load current response is shown for sample A in figure 12. The response for this configuration evidently follows the time derivative of the incident field. Reflections are observed at expected times and are related to the electrical length of the sample.

Parameters for sample A and the PPF impressed field were used as input data for the NLINE computer program. Results of the computations are shown in figure 12 for three angles of incidence. The ψ = 0 curve corresponds to the experimental conditions in the PPF. The incident electric field amplitude, 35.5 V/m, resulted in a measured peak induced voltage of -100 mV at the loads. That the induced voltage computed by NLINE is also -100 mV indicates that computer modeling of sample A was accurate.

The remaining curves in figure 12 show the variation in induced voltage as the angle of incidence is changed. The time shift for the starting point of the plots arises from phase terms in the numerical Fourier transform used in NLINE. No effort was made to eliminate this, since the amplitude and waveshape would remain unchanged.

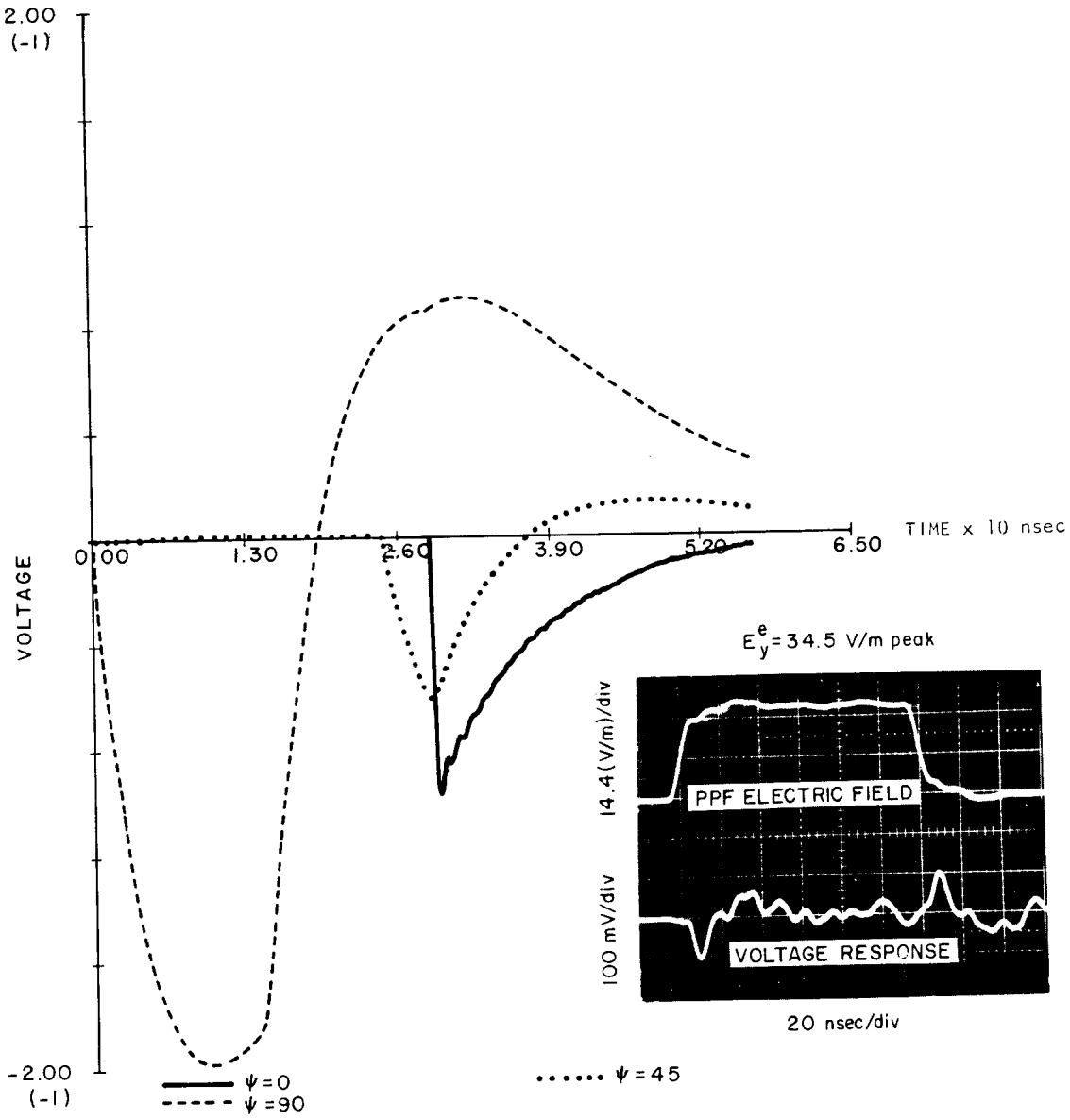

Figure 12. Voltage response of sample A at ψ = 0, 45, and 90 deg with experimental data at ψ = 0 deg.

Additional numerical results are shown for sample A in figure 13, where the angle of incidence is 90 deg, and the point of computation is varied along the length of the transmission line. The voltage is zero at the center ($x = \ell/2$) because of symmetric terminations. The current is at a maximum at this position. Such voltage and current occur because the terminating 100-ohm resistances are lower in value than the characteristic impedance of sample A (about 200 to 300 ohms) and thus tend to act like short circuits for this configuration.

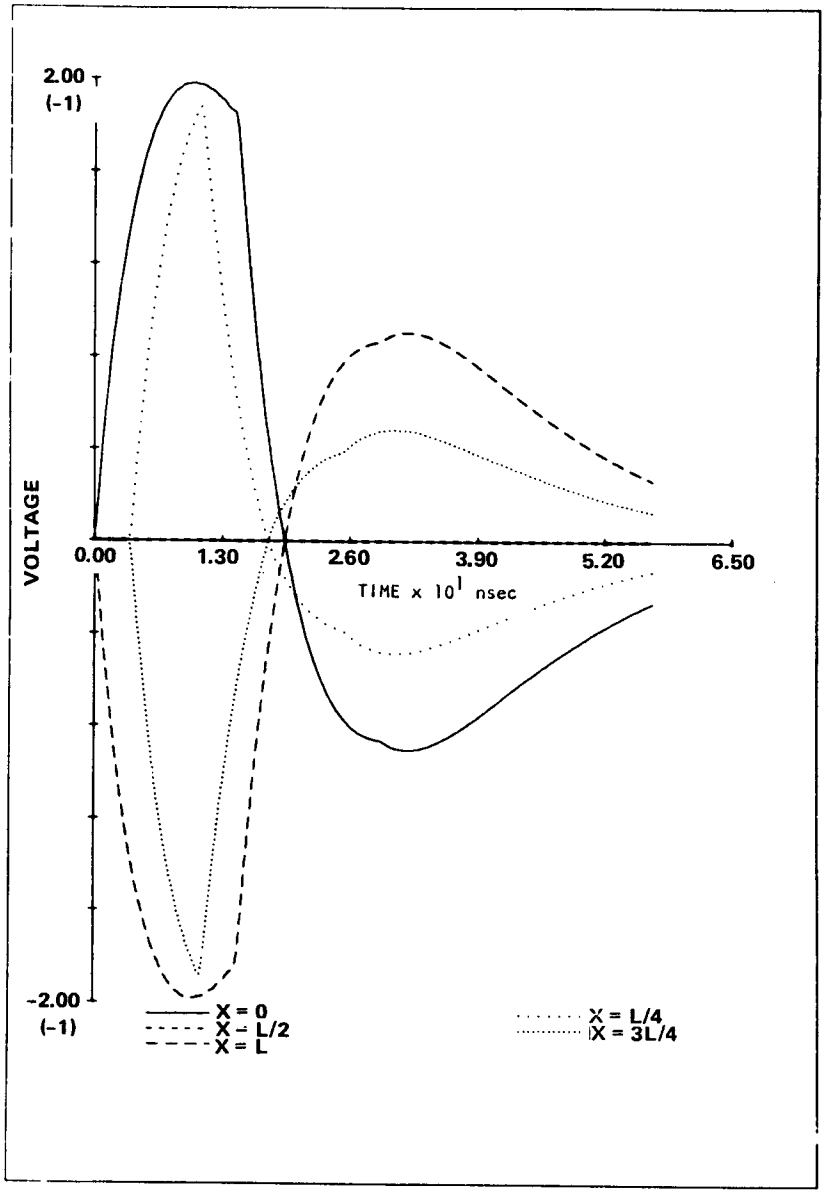

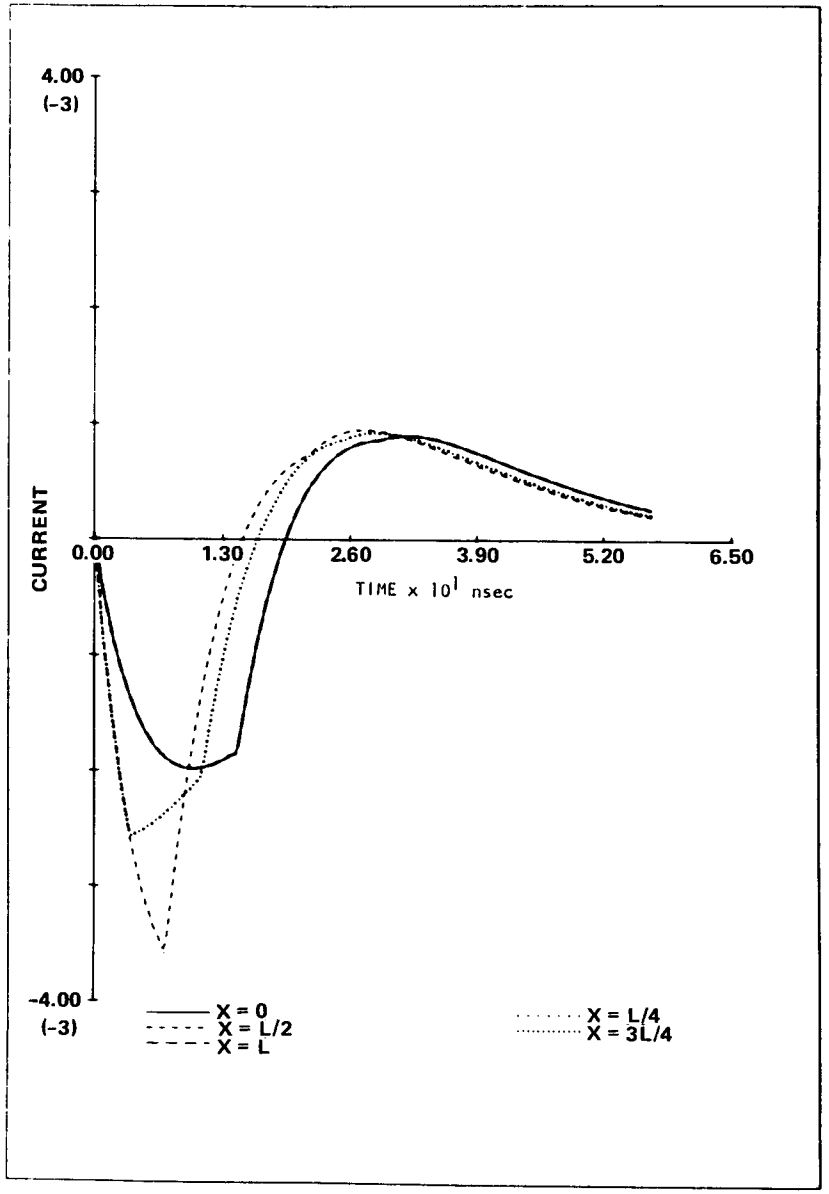

Figure 13. Voltage and current response of sample A at several x-axial positions along the conductors, ψ = 90 deg.

Similar PPF measurements and NLINE computations were made on sample B. Figure 14 shows the conductor cross section and a composite plot of the computed voltages induced on each conductor, by use of an impressed field pulse shape and amplitude similar to the experimental conditions. The time delay and initial noise are introduced by the Fourier transform subroutine. The end-on $\psi = 0$ deg angle of illumination is a critical angle in the lossless TEM mode theory and results in a computed rise time that is faster than observed in the experiments. Inhomogeneous dielectric conditions and conductor proximity effects can be expected to add further complications. The purpose is, however, to test the adequacy of the theory on a relatively nonideal sample, since most transmission lines in use fall into this category from the analysis.

Figure 15(a to j) shows numerical and experimental results for sample B. Computed results are given in both the frequency and time domains. The actual measurements and peak induced voltage values are shown in each part of figure 15.

The thin wire approximations and the potential coefficients were used to determine the coupling parameters for the NLINE computer runs. These values were observed to be considerably higher than the measured values, as was shown in figures 9 and 11. This difference is important in comparison of computed and measured results. The computed peak voltages are consistently larger than the measured voltages because of the larger value for coupling parameters used. Peak value and rise time degradation can also be expected in an experiment, due to instrumentation and nonideal coupling. The existence of non-TEM modes was observed in the measurements. However, when ratios of measured-to-measured values are used for the coupling parameters in reducing the computed peak values, the experiment and theory are compatible within factors ranging from 1.1 to 9. Best agreement by this analysis is obtained for conductors 1, 2, 3, 4, 5, and 7. Results for the remaining conductors are off by factors of 4 or more and require further refinement in the semi-empirical approach. The peak values of computed time domain voltages were reduced as suggested above by the ratios of measured-to-computed values of the Maxwell's capacitance coefficients and magnetic field coupling parameters obtained from figures 9 and 11. These reduced values appear in parentheses next to the peak of each computer plot in figure 15(a to j). These values correspond to use of measured $\underline{C}$ and $\underline{L}^e$ as inputs to NLINE. Evidently much better agreement is obtained.

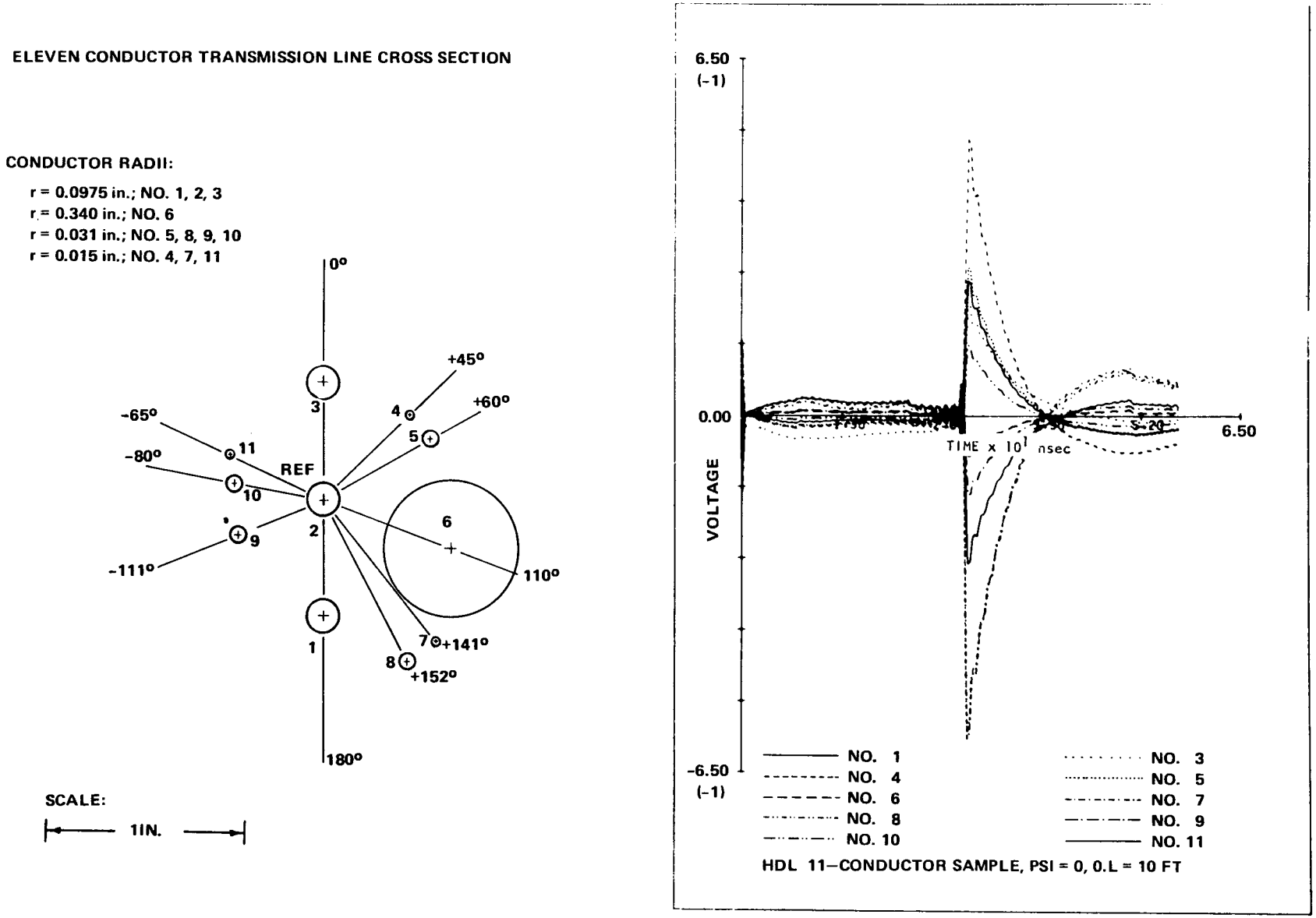

Figure 14. Sample B: composite results from the NLINE computations, ψ = 0 deg.

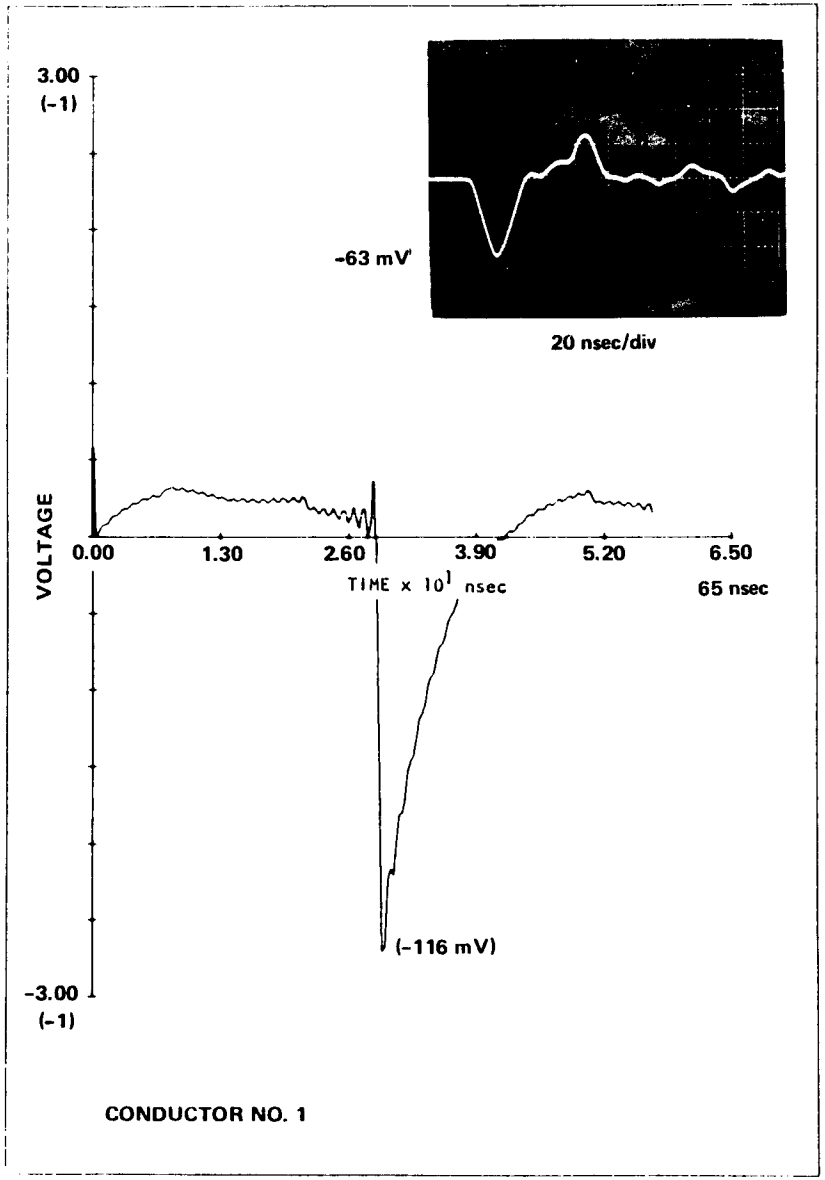

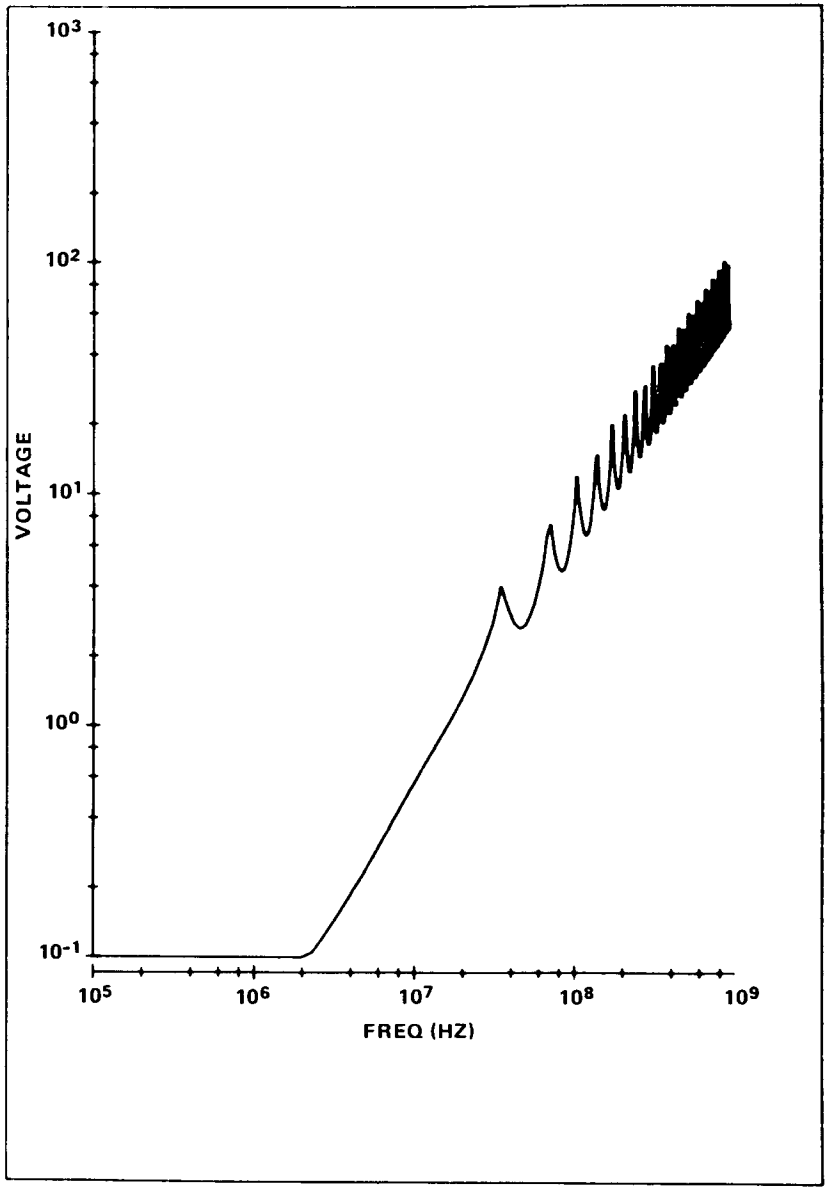

(a)

Figure 15. Sample B: numerical and experimental results.

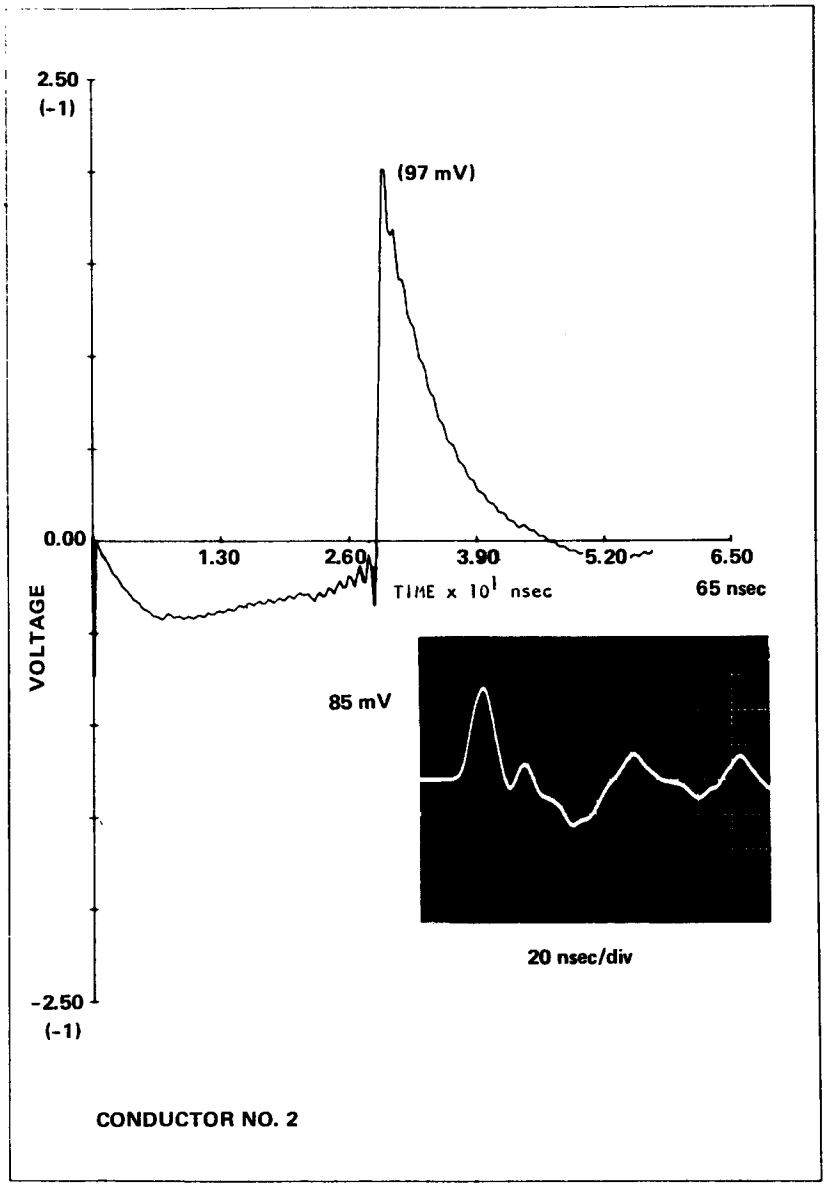

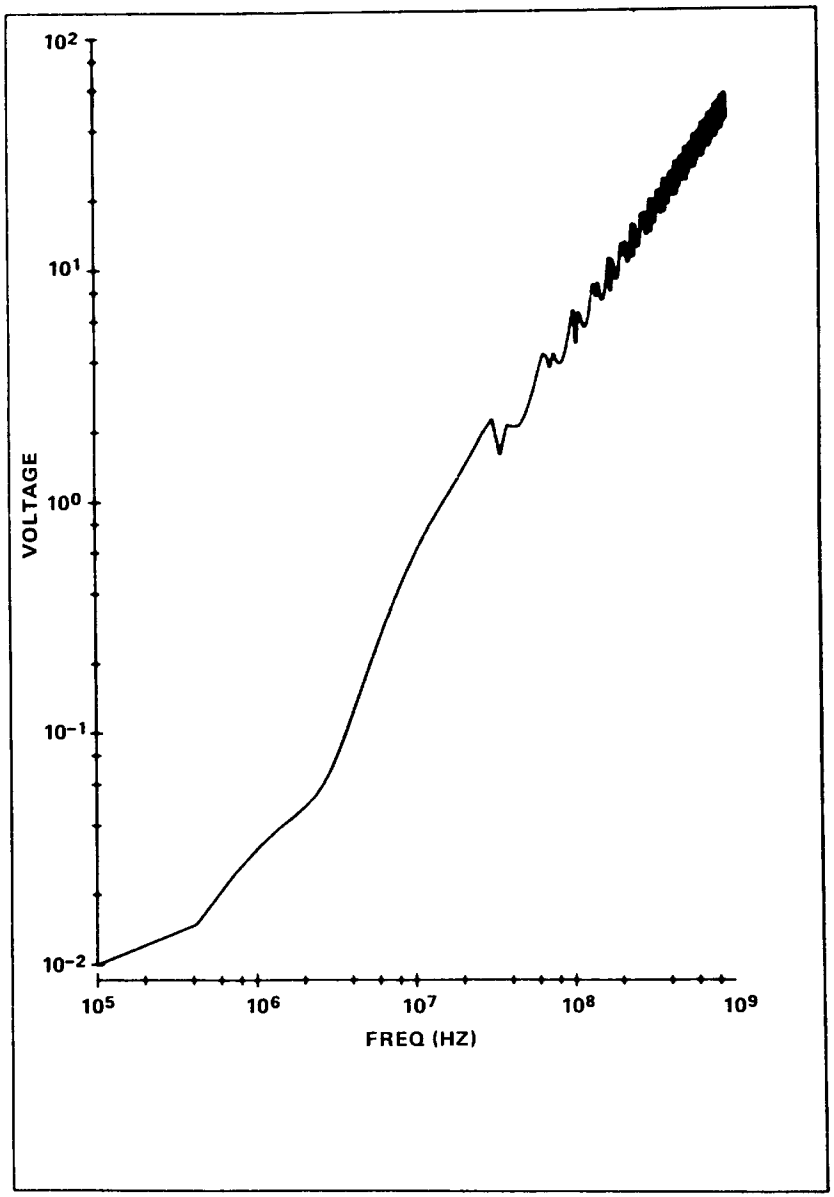

(b)

Figure 15. Sample B: numerical and experimental results. (Cont'd)

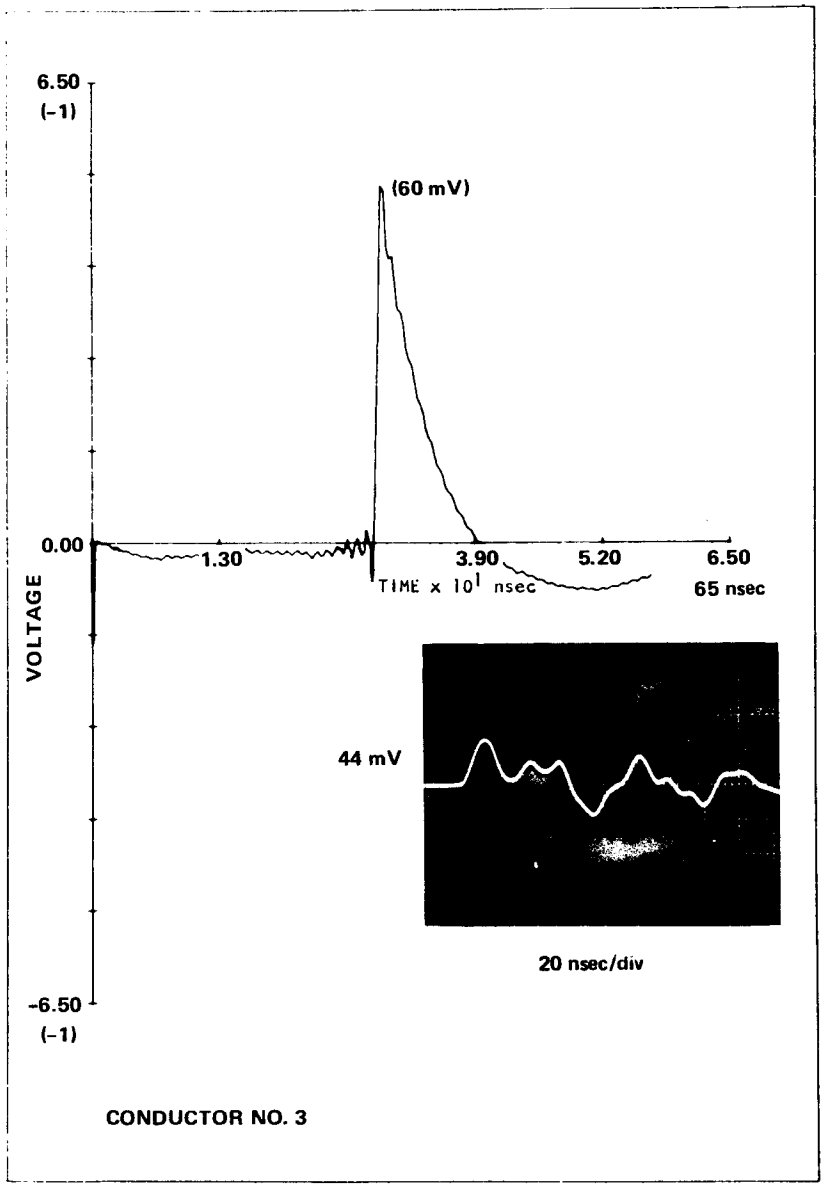

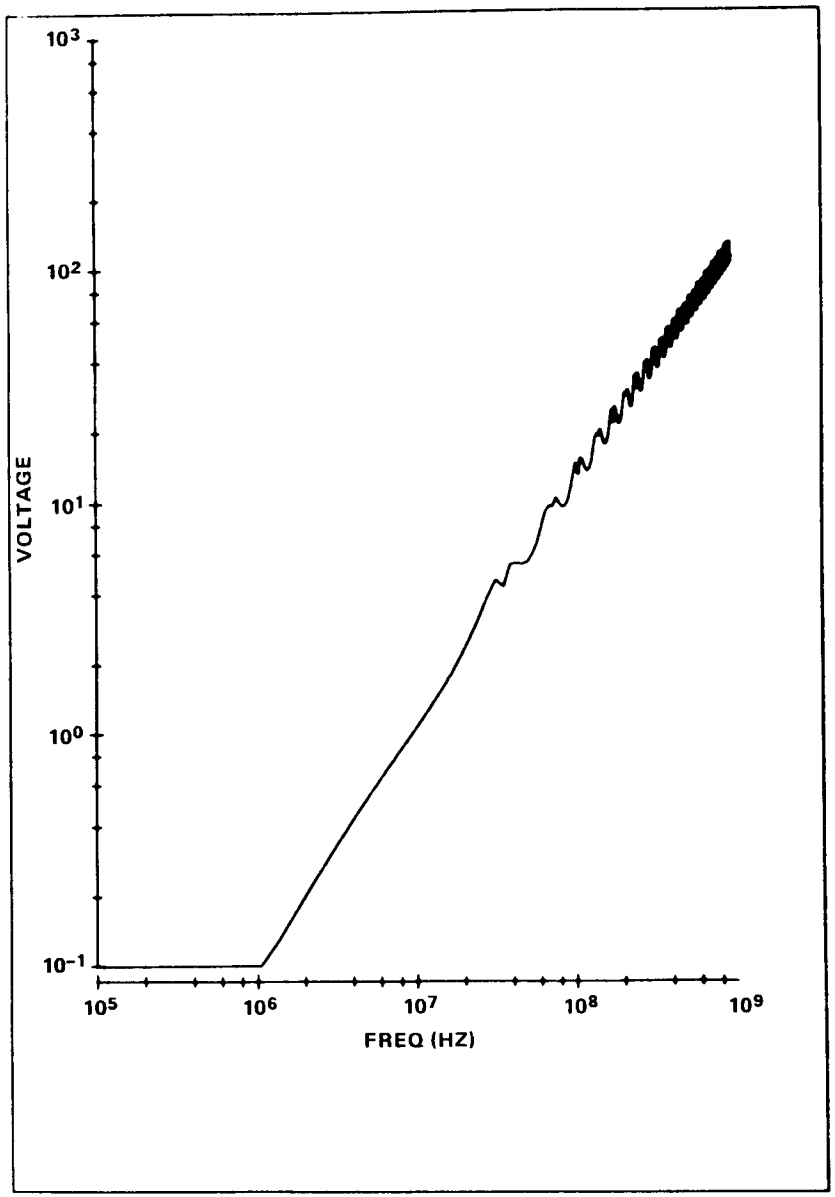

(c)

Figure 15. Sample B: numerical and experimental results. (Cont'd)

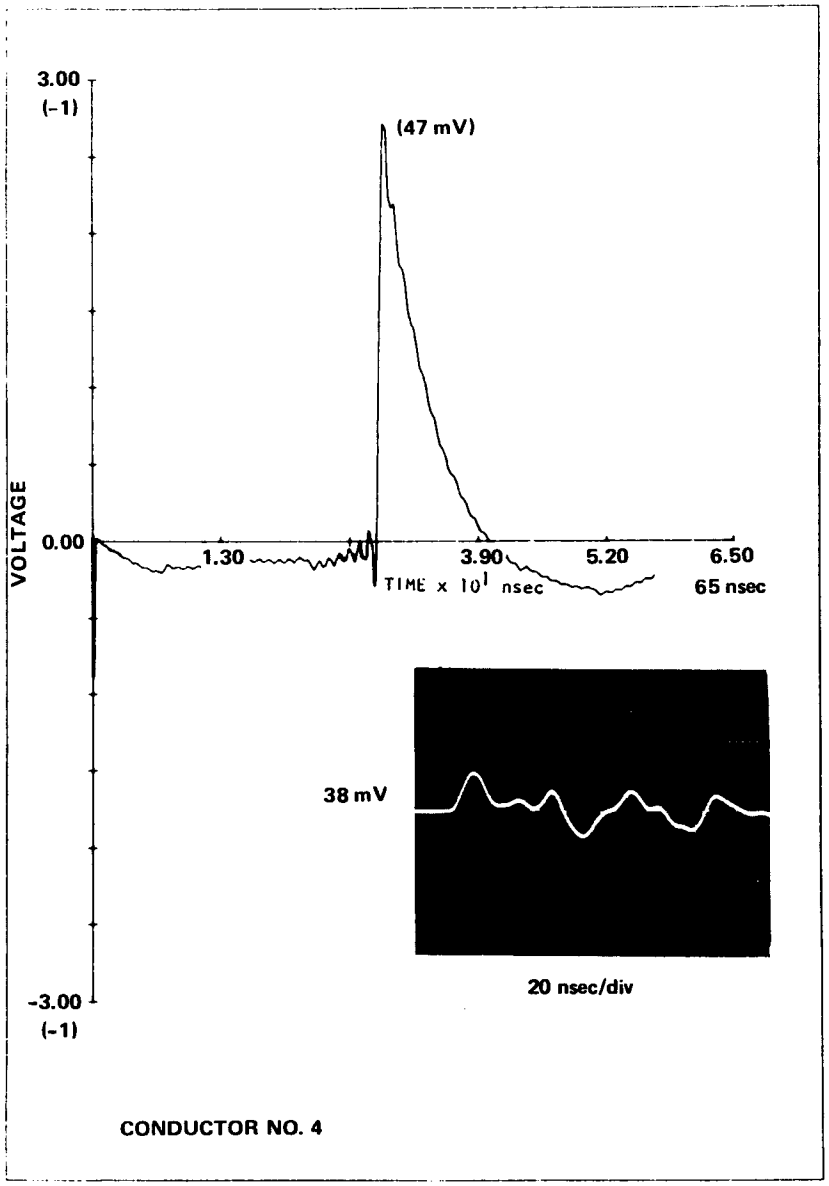

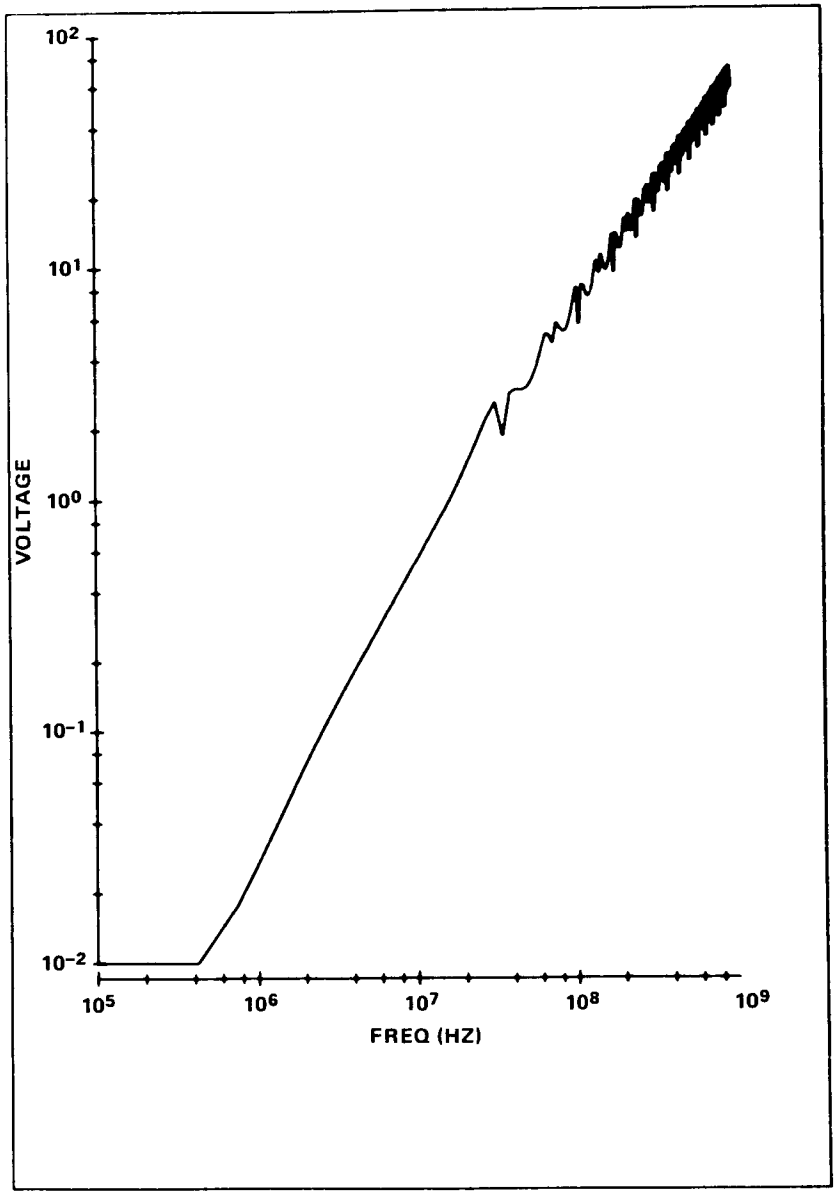

(d)

Figure 15. Sample B: numerical and experimental results. (Cont'd)

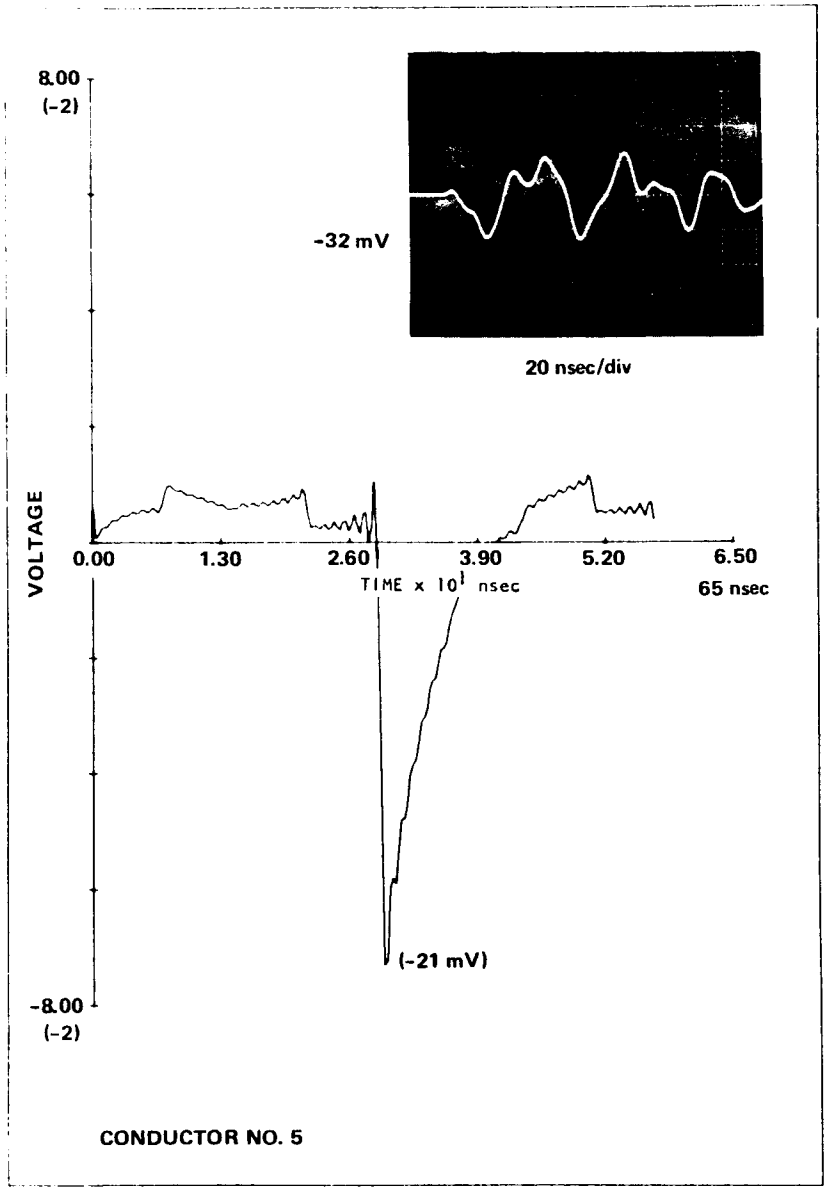

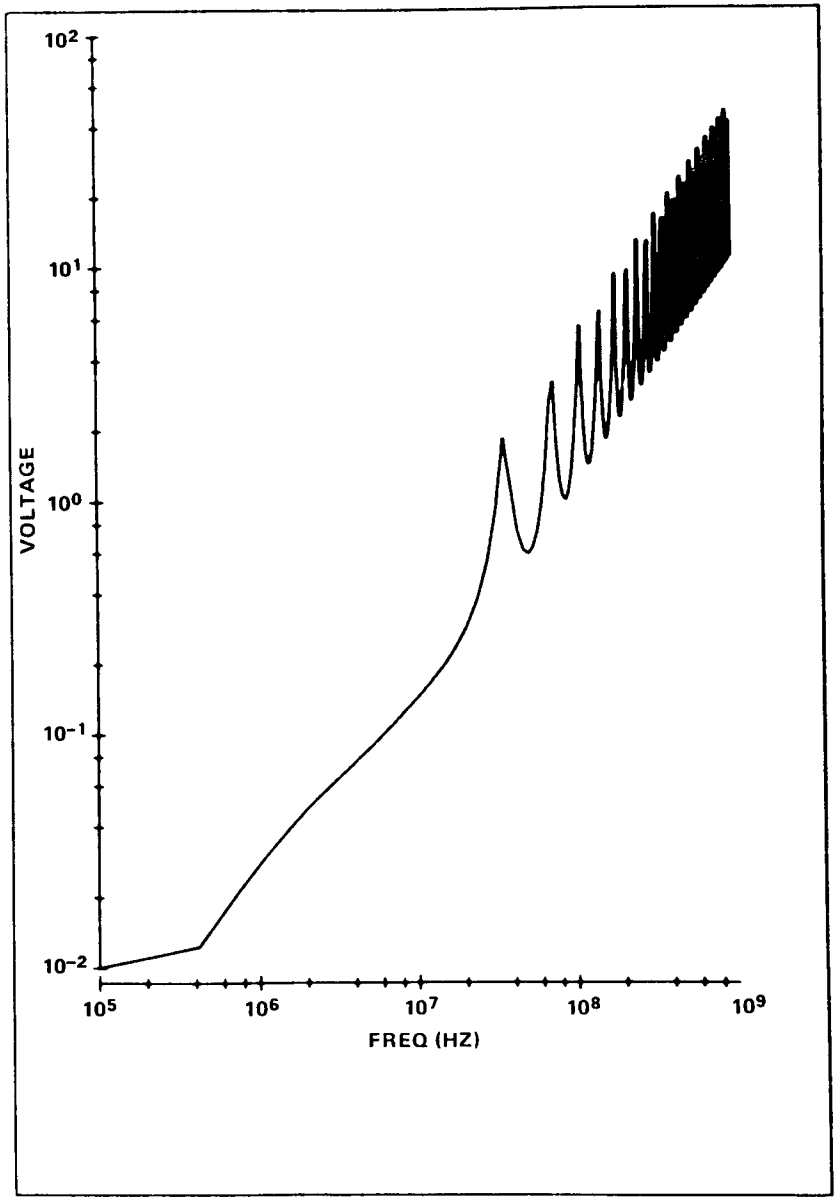

(e)

Figure 15. Sample B: numerical and experimental results. (Cont'd)

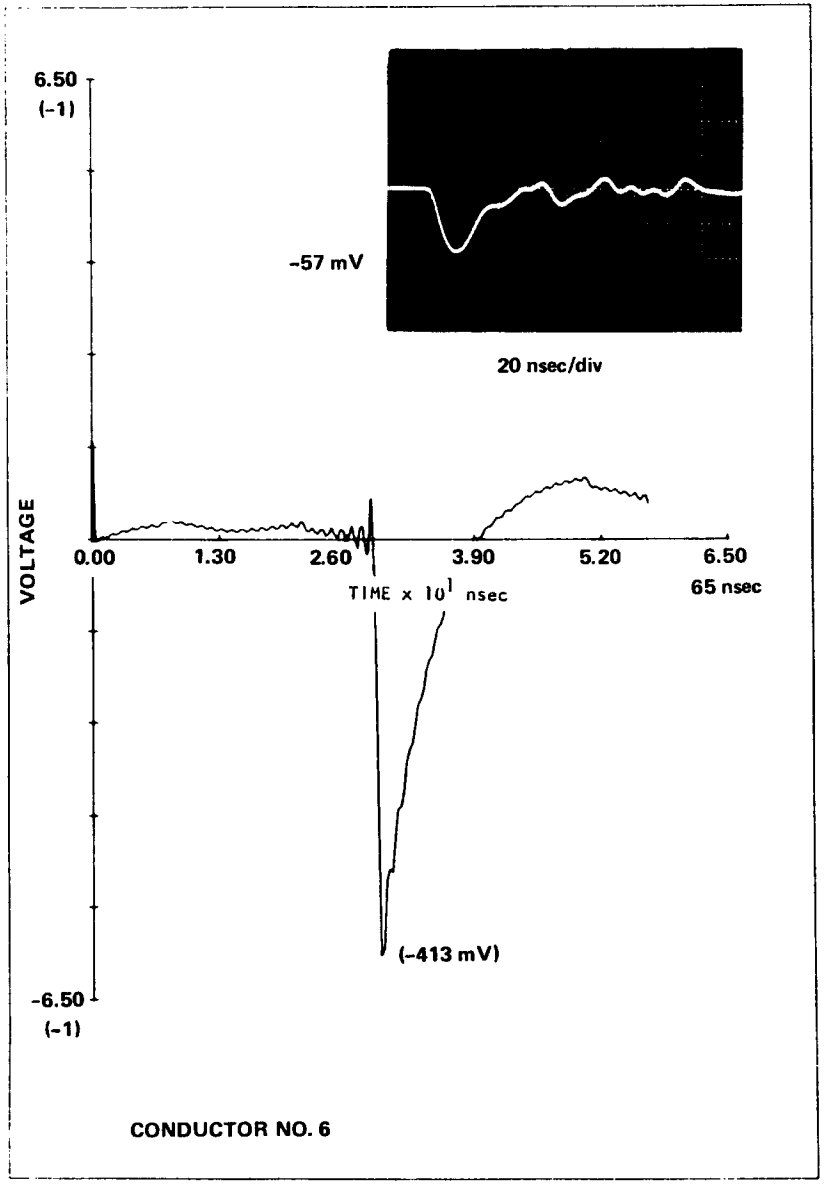

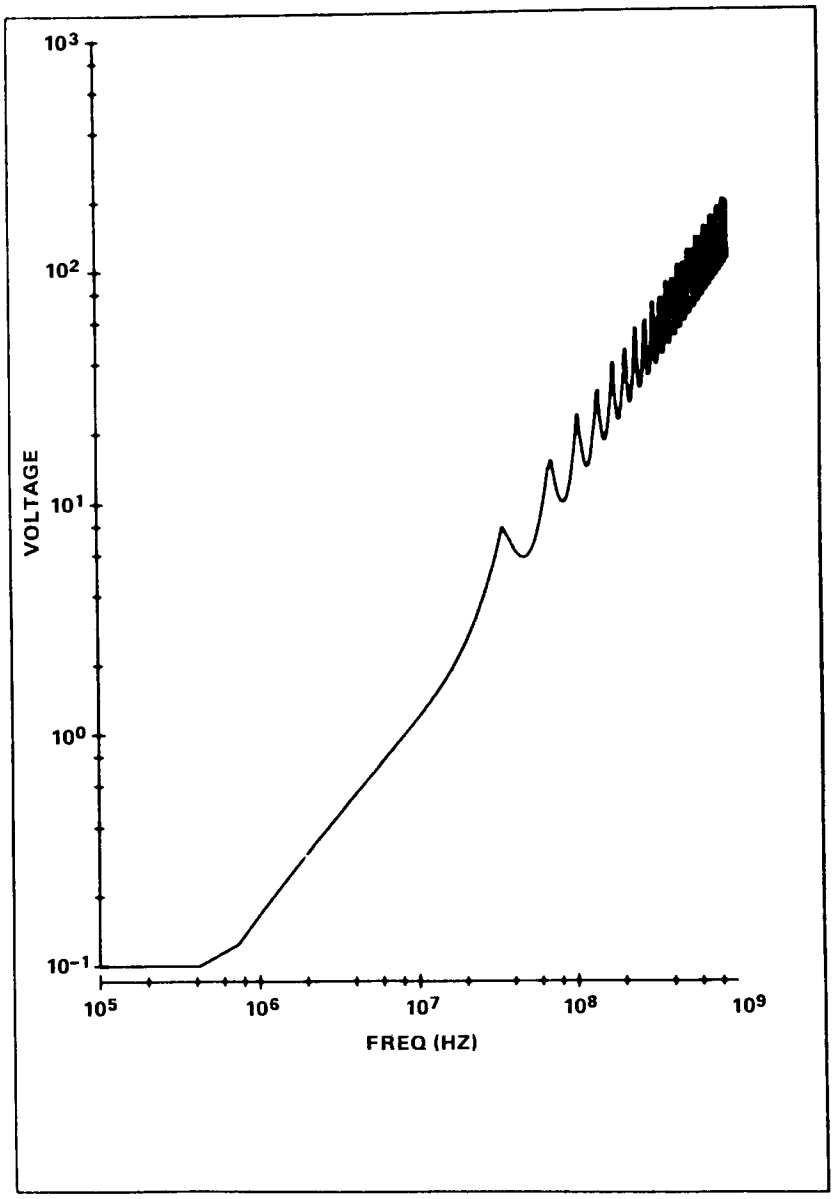

(f)

Figure 15. Sample B: numerical and experimental results. (Cont'd)

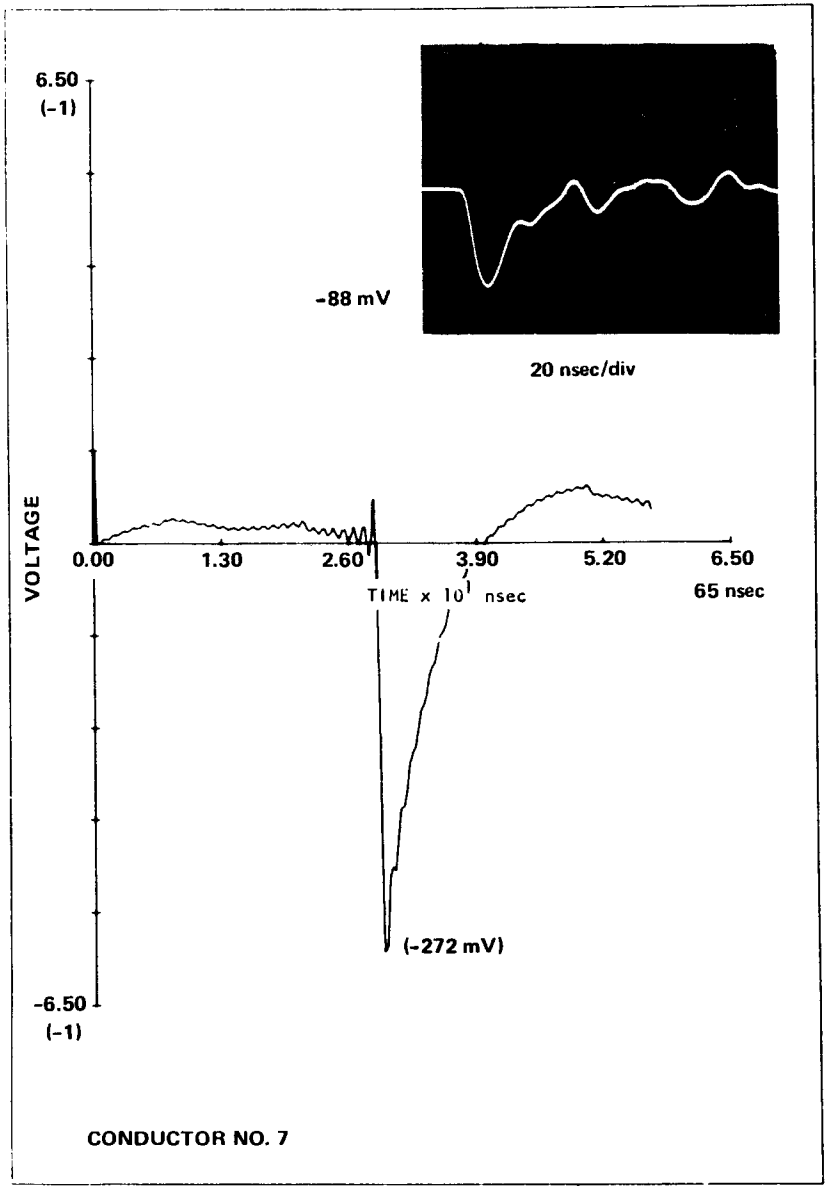

(g)

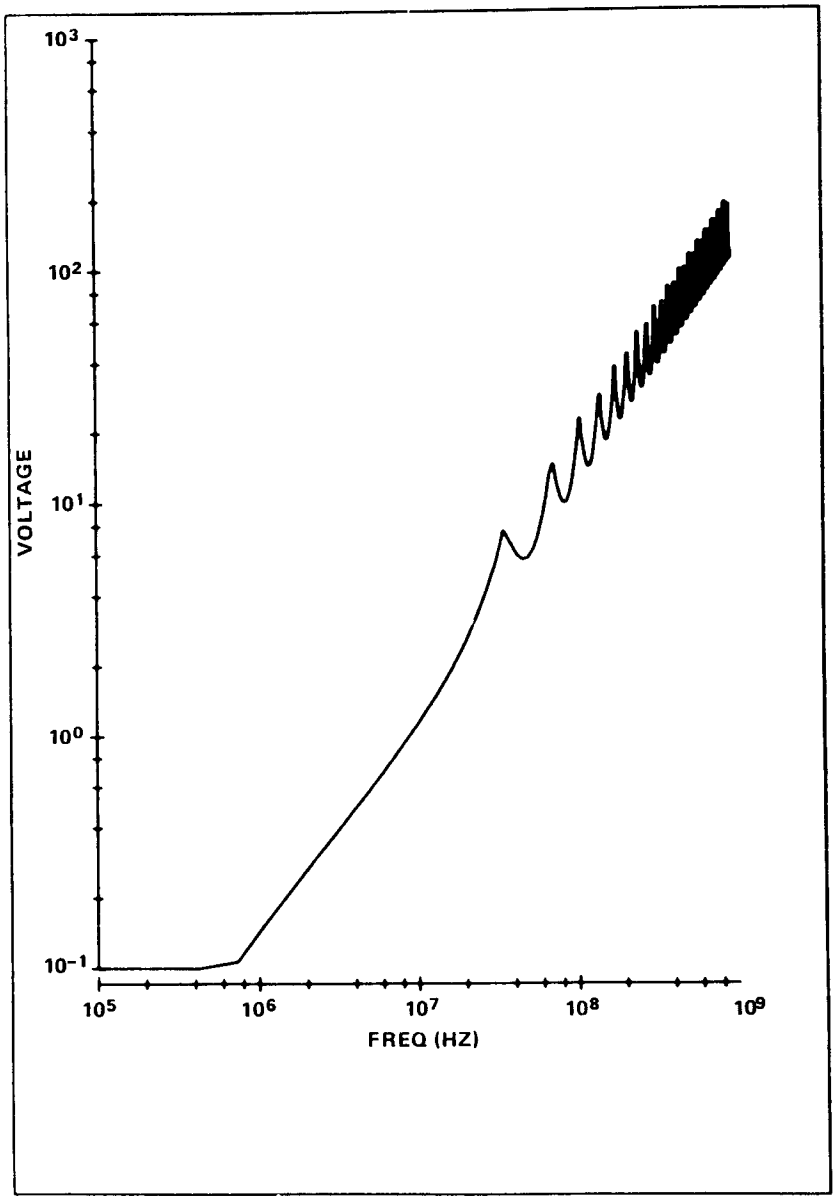

Figure 15. Sample B: numerical and experimental results. (Cont'd)

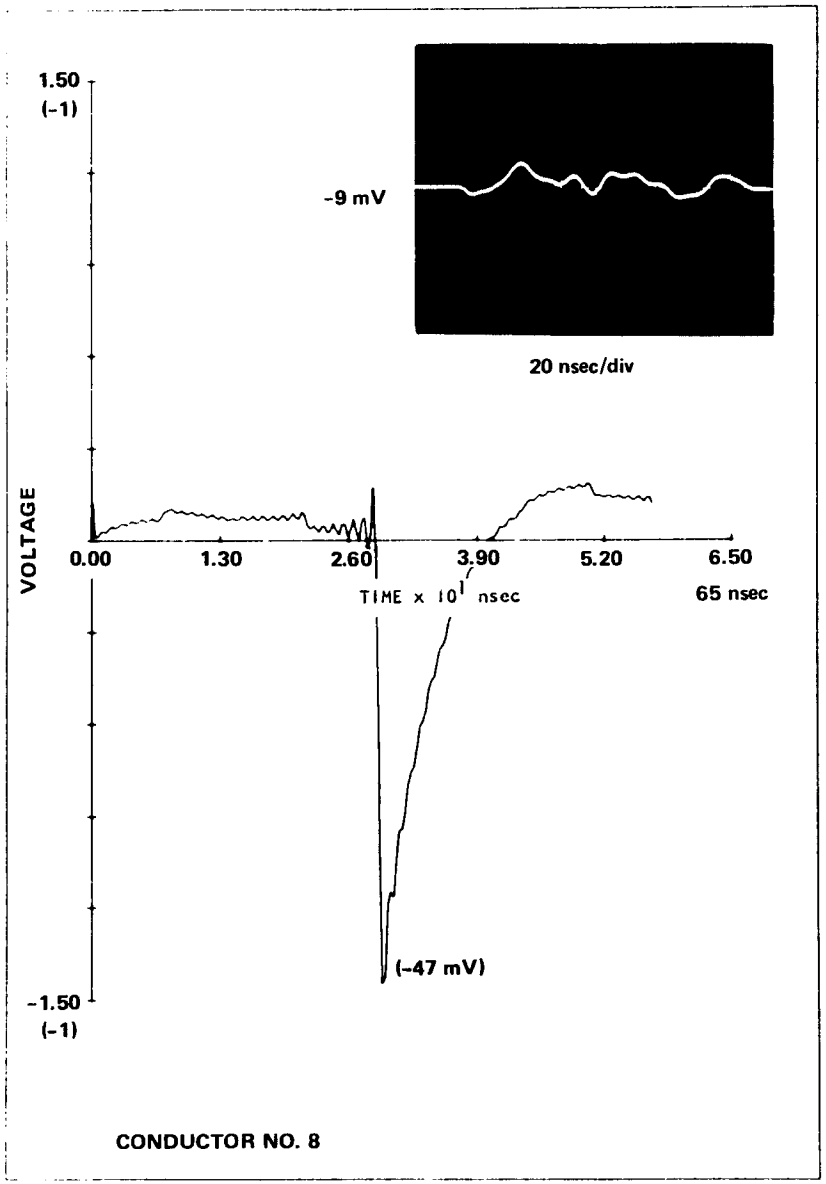

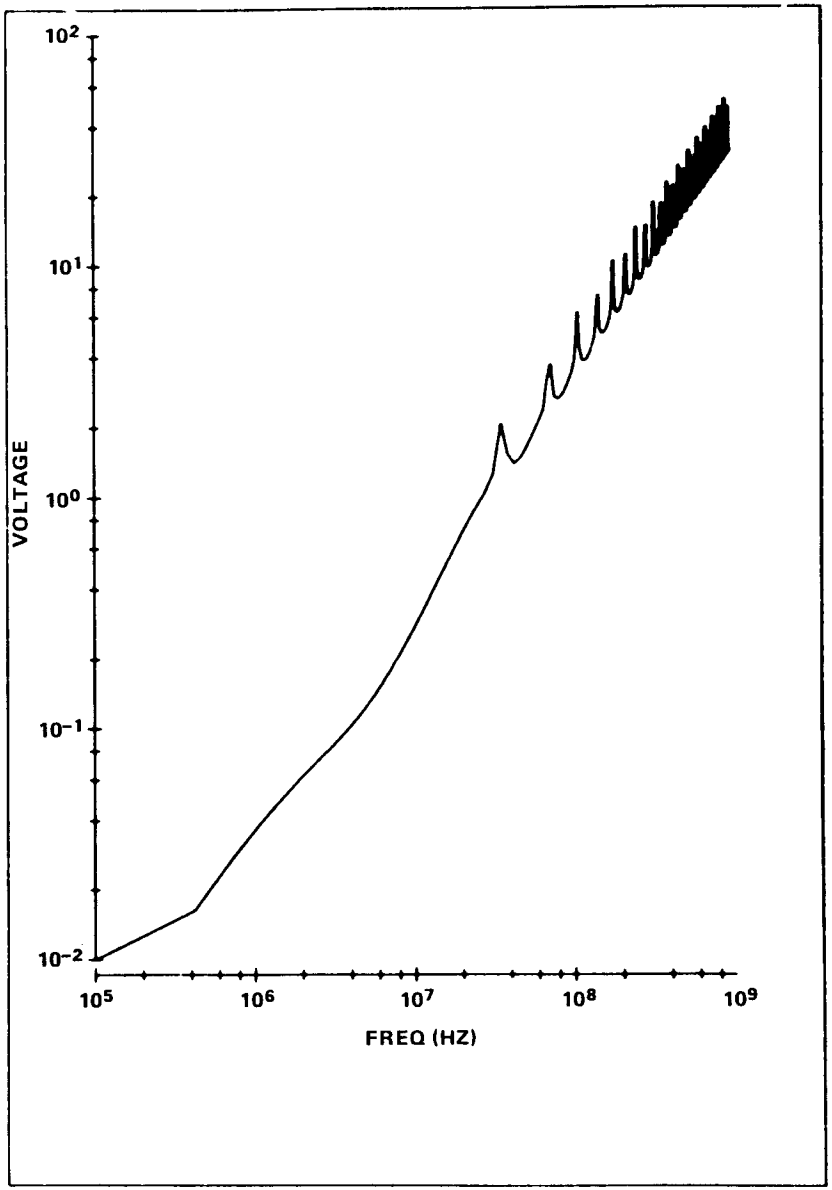

(h)

Figure 15. Sample B: numerical and experimental results. (Cont'd)

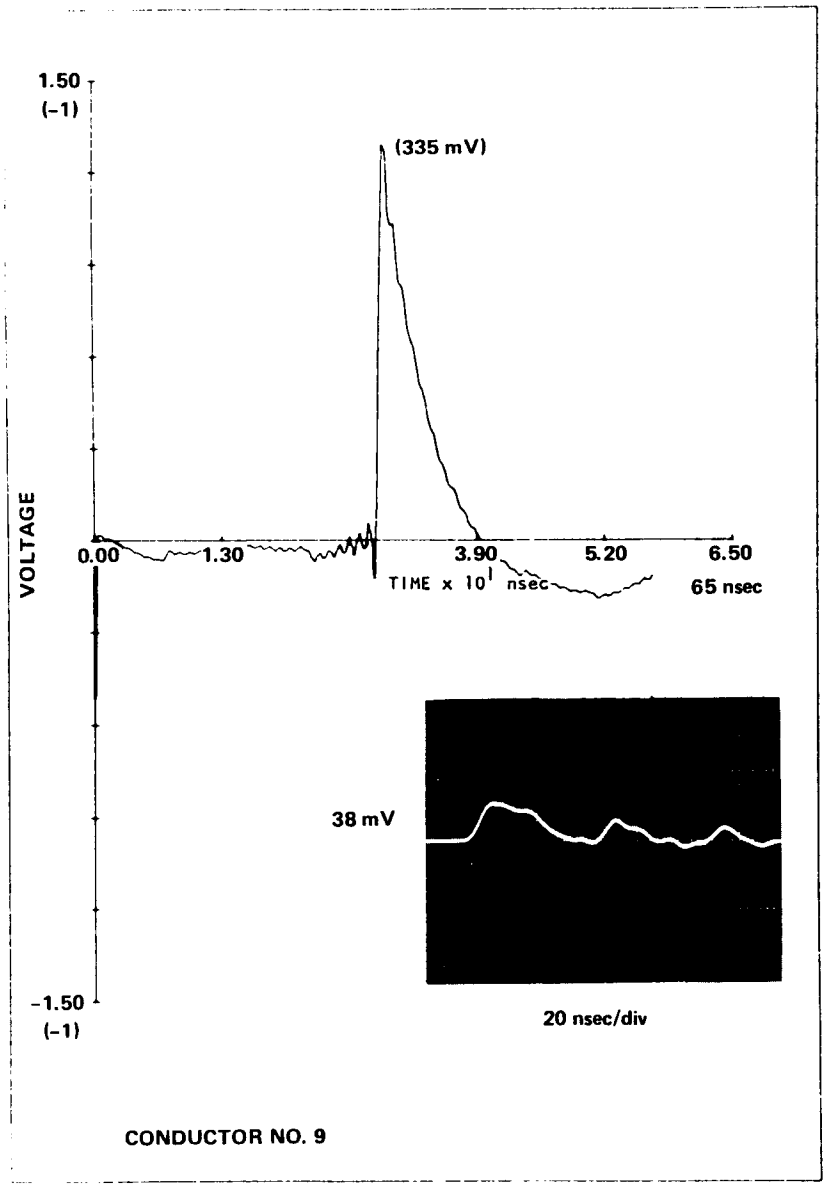

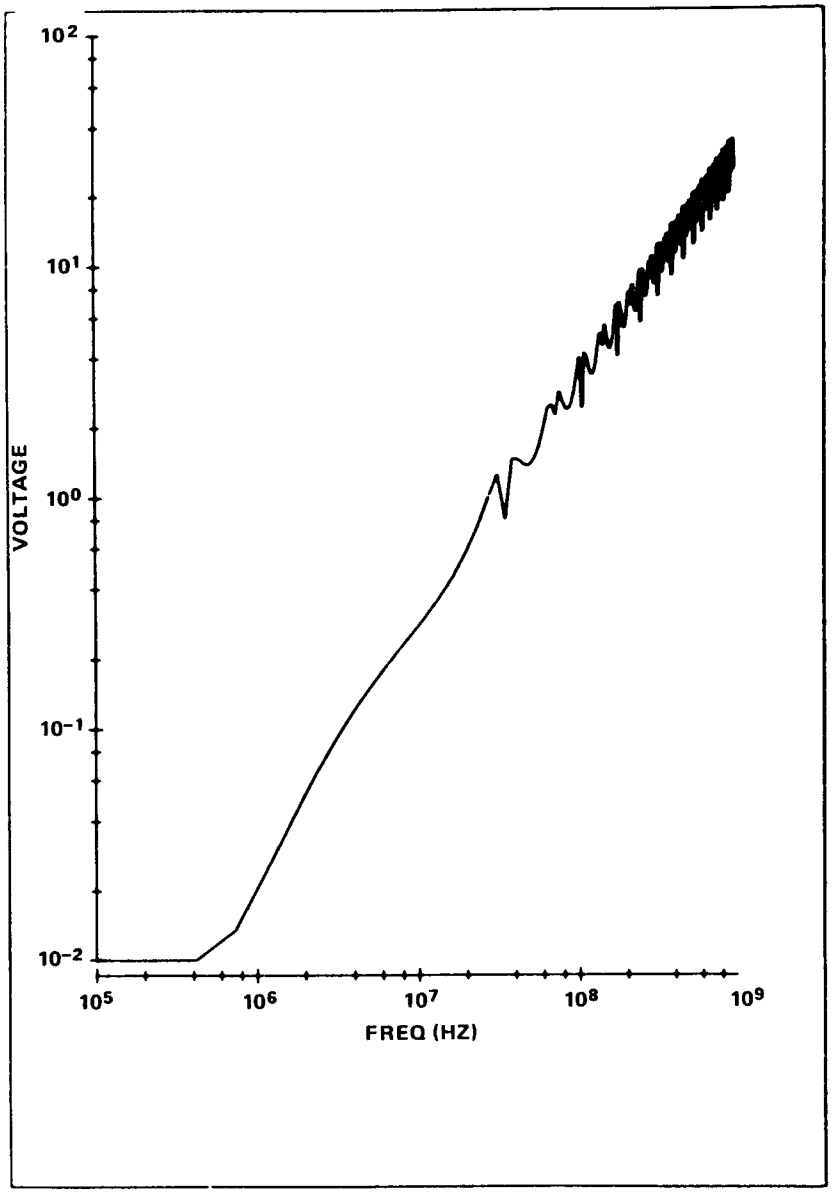

(i)

Figure 15. Sample B: numerical and experimental results. (Cont'd)

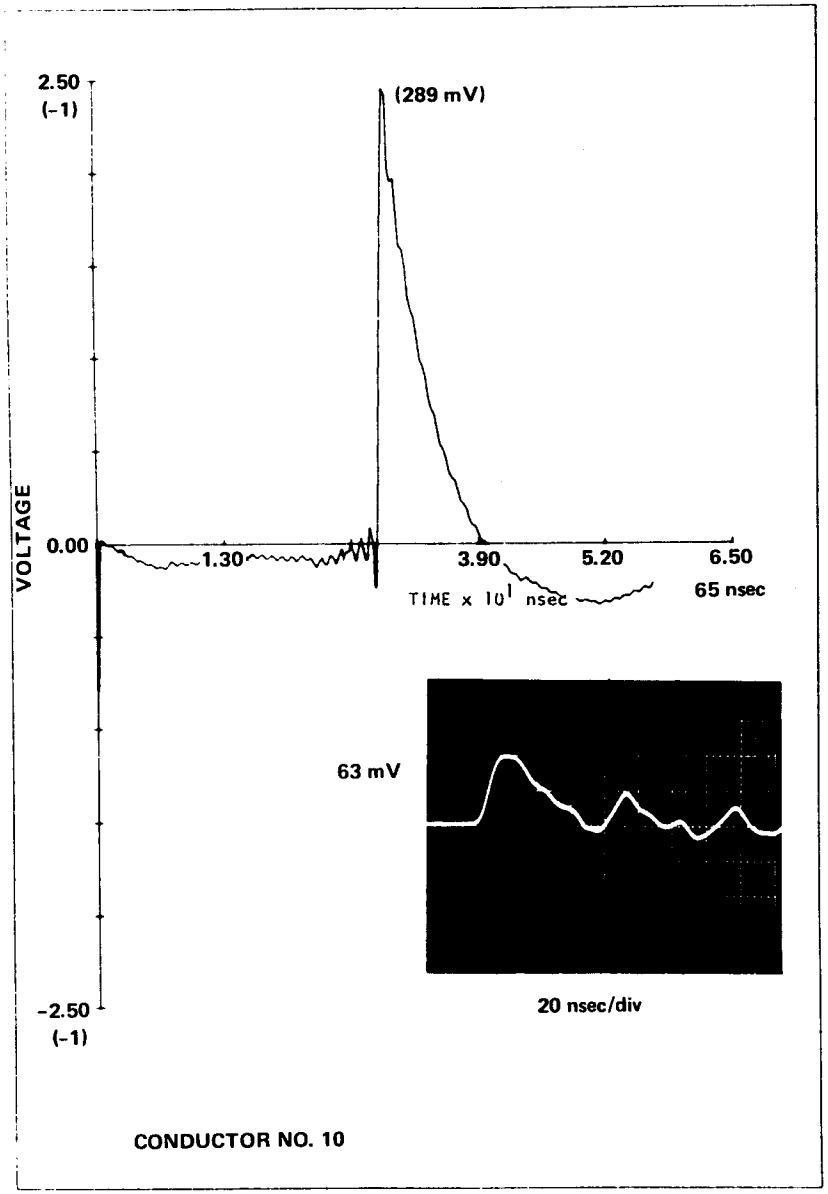

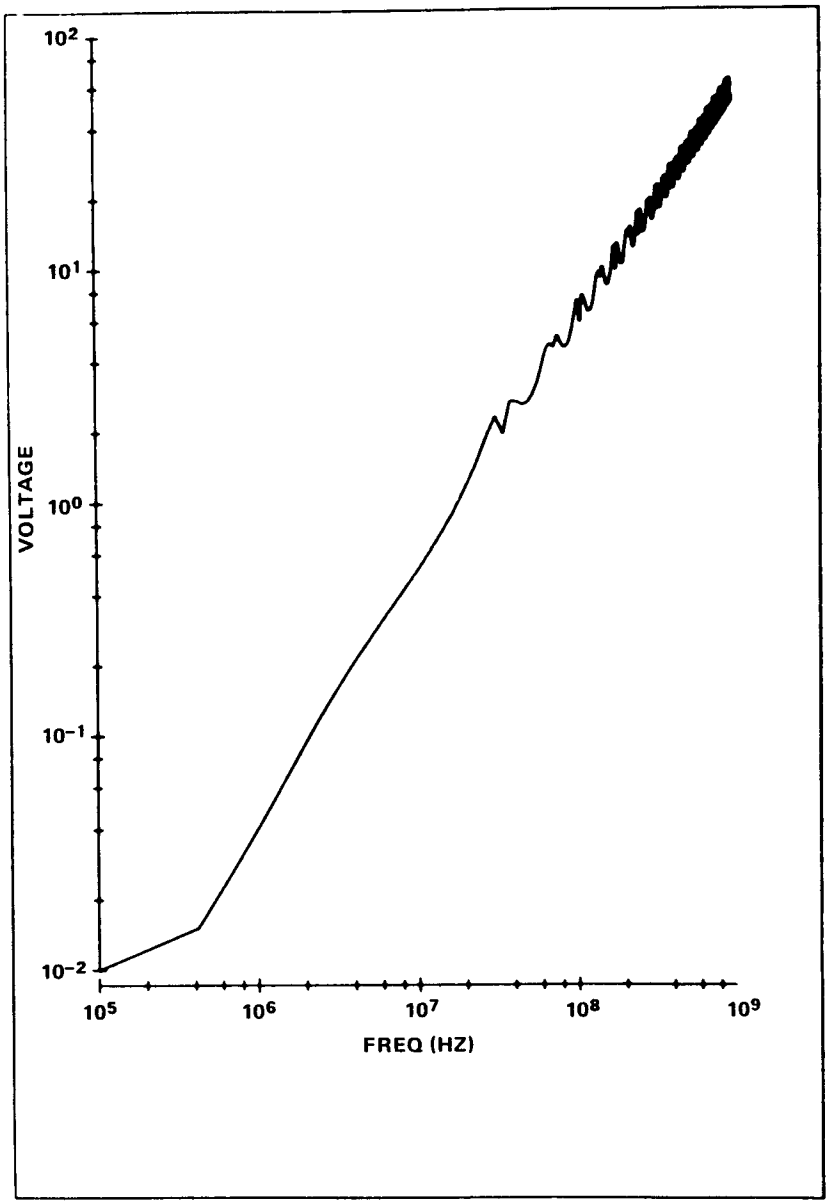

(j)

Figure 15. Sample B: numerical and experimental results. (Cont'd)

10. CONCLUSIONS

The numerical and experimental procedures developed in the course of this work provide a versatile tool for analysis of electromagnetic coupling with multiconductor transmission lines. The NLINE computer program has been tested for many configurations. In the present form, the program is dimensioned in FORTRAN to work with samples containing up to 11 conductors. Dimensioning can be increased when more conductors are considered.

Procedures for determination of the coupling parameters were established. More effort is required in measurement of the off-diagonal mutual capacitance coefficients. A capacitance bridge or similar instrumentation could be used.

The thin wire approximations work best for the simpler geometries, but can be applied with proper judgment to the complex conditions, also. It was found experimentally that conductor separations in the order of two or three diameters are sufficient to approach thin wire conditions, as can be demonstrated easily for the two-conductor transmission line, since an exact solution to Laplace's equation is available.

The voltage and current response is sensitive to angle of incidence of the field and to terminating impedances, as was demonstrated by NLINE computations and PPF measurements. For example, impedances that had been varied at one end of sample A caused voltages and currents to vary from positive, zero, and negative values when the angle of incidence was end-on (ψ = 0 deg). The transmission line can be made to respond as a directional coupler in this configuration. configuration.

As in many complex problems, exact agreement between theory and experiment cannot always be obtained. The simpler configurations tend to give the best results. A greater amount of analysis is required for the complex conditions. For this purpose, the NLINE computer program and the experimental techniques developed in this study can be applied.

ACKNOWLEDGEMENTS

The author thanks S. Frankel and J. Bombardt for helpful suggestions and L. Ambrose for the experimental work.